

## 国際化推進共同研究概要

No. 1

タイトル: Electron heating of QUEST start-up plasmas, with and without coaxial helicity injection.

研究代表者: Taylor, Gary

所内世話人: 出射 浩

研究概要:

米国、プリンストン・プラズマ物理研究所では、NSTX 装置で CHI による非誘導プラズマ電流立ち上げの際、電子温度が低いため、電子サイクロトロン加熱による追加熱が検討されている。QUEST 装置で、同様に CHI による非誘導プラズマ電流立ち上げ、さらに電子サイクロトロン加熱による非誘導プラズマ電流立ち上げが行われている。QUEST 装置で、CHI 単独、電子サイクロトロン加熱単独の非誘導プラズマ電流立ち上げが行い、各々有効な電流立ち上げを確認した。

## Electron heating of QUEST start-up plasmas, with and without Coaxial Helicity Injection

Gary Taylor

*Princeton Plasma Physics Laboratory, Princeton, NJ, U.S.A..*

A long-term goal of the National Spherical Tokamak Experiment Upgrade (NSTX-U) at the Princeton Plasma Physics Laboratory (PPPL) is non-inductive start-up of plasmas with 28 GHz electron cyclotron heating (ECH) and electron Bernstein wave heating (EBWH). Prior to the recent major repair of NSTX-U Coaxial Helicity Injection (CHI) was also being planned for non-inductive start-up on NSTX-U, with the addition of ECH when it became available, but with the planned removal of the electrical break required for CHI this will no longer be possible in the future. QUEST has 28 GHz and 8.56 GHz heating and CHI, so a collaboration between PPPL and QUEST researchers on the topic of non-inductive start-up scenarios that use ECH, ECH + CHI and EBWH to start-up the QUEST plasma non-inductively would greatly benefit the planning of these future NSTX-U start-up experiments and it would provide an opportunity for NSTX-U researchers to learn how to implement and program non-inductive start-up discharges.

Non-inductive plasma start-up with high density and current is a key issue for advanced tokamak reactor concepts as well as for the spherical tokamak concept. The ECH system with a 28 GHz gyrotron has been prepared for non-inductive electron cyclotron (EC) plasma ramp-up in the QUEST. There are two important aspects of conducting the present ECH current ramp-up experiments. One is beam focusing, and the other is incident polarization control. All elliptical polarization states can be controlled in combination with two corrugated directions of the polarizers with respect to incident planes of the waves. Two corrugated plates were designed and fabricated with careful attention to reduce Ohmic losses by means of high-precision milling, not wire-electrical discharge machining [1]. The two-mirror launcher system has been developed to obtain a narrow beam size of  $w \sim 0.05$  m. The mirror area should cover the 1% intensity edge of  $1.5w$  in the beam. The final 2<sup>nd</sup> focusing-mirror diameter was 0.37 m for sharp beam focusing. Considering the principle of the least propagating-phase, the Kirchhoff integral and the Gaussian optics were used to evaluate mirror surface design by analyzing the propagating-phases before and after the first mirror reflection, respectively. The incident beam can be steered from perpendicular to tangential injections. The steering capability with focusing property was confirmed at the low power test facilities.

The local ECH effect was confirmed with incident polarization scanning by rotating the corrugated polarizer-plates. The 140 kW 28 GHz-wave with a parallel refractive index  $N_{//} = 0.78$  at the 2<sup>nd</sup> harmonic ECR layer was obliquely injected into the QUEST. The ramped plasma current ( $I_p$ ) was observed on the incident polarization. The experiment with each polarization was conducted after a shot with the default polarizer-angle setting to ramp up  $I_p$  normally. The  $I_p$  ramp up was observed to depend on the incident polarization, indicating the local ECHCD effect. Although 140 kW

power could be transmitted with no arcing events, arcing events were frequently detected at the polarizer section with higher transmitted power. Therefore, a new quasi-optical concept for the polarizer system was proposed to avoid the arcing, and successfully implemented for higher power injection.

Figure 1 shows the time evolution of  $I_p$ , the loop voltage, poloidal coil currents ( $I_{PF}$ ), the  $H\alpha$  intensity, absolute extreme ultra violet (AXUV) bolometer signal, electron density ( $n_e$ ) and temperature ( $T_e$ ), and the hard X-ray (HX) count and energy, with 230 kW 28 GHz-wave of  $N_{||} = 0.78$  at the 2<sup>nd</sup> harmonic ECR layer. The 20 kW 8.2 GHz-wave was also used for plasma pre-ionization. The plasma current reached 80 kA, following the poloidal field ramp-up at zero or negative loop voltages. The electron density and temperature were measured by Thomson scattering diagnostics at a major radius  $R = 0.34$  m, which is near the 2<sup>nd</sup> ECR layer of  $R_{res} = 0.32$  m. A relatively high-density plasma (at  $n_e \sim 2\text{-}6 \times 10^{18} \text{ m}^{-3}$ ) was obtained in comparison with the previous experiments with no beam focusing [2]. The right-hand cut-off density  $n_{cut}$  of the 2<sup>nd</sup> harmonic 28 GHz-wave is  $2.4 \times 10^{18} \text{ m}^{-3}$  at  $R = 0.34$  m for oblique injection with  $N_{||} = 0.78$  at the ECR layer. The temperature  $T_e$  decreased with the increasing  $n_e$  beyond  $n_{cut}$ , then the HX count started to increase. The HXs with a 60 keV energy range were measured at the forward tangential viewing radius of 0.32 m for current-carrying electrons. The maximum relativistic Doppler shift resonance radius  $R_D$  was evaluated as 0.406 m. The local ECH effect with the focused beam was limited within an inboard region of  $R \leq R_D$ . The multiple reflection effect should be dominant where  $R > R_D$ , after the incident beam was reflected at the cut-off. The generated energetic electrons may contribute to the current ramp-up.  $I_p$  suddenly dropped around  $t \sim 3.09$  s with sharp rises in the AXUV signal and the  $H\alpha$  intensity. The mechanisms causing the  $I_p$  ramp-up and drop will be investigated by controlling the local ECH effect through scanning of the incident polarization and  $N_{||}$ .

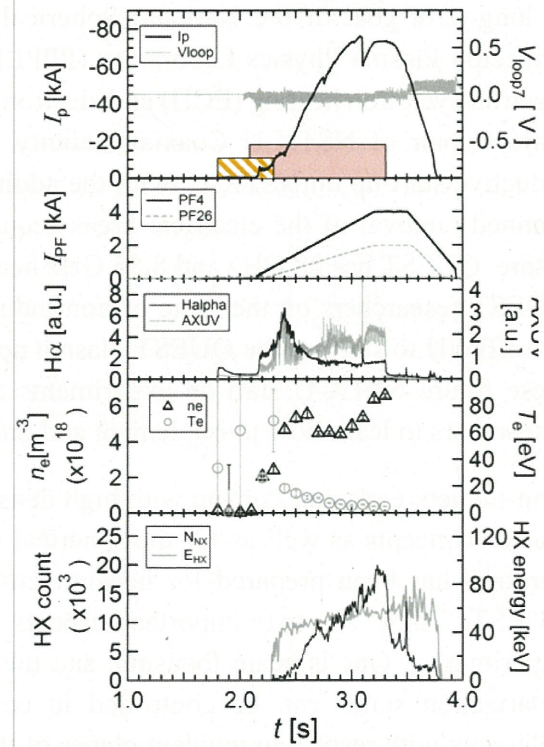


Fig. 1: Time evolution of the plasma current  $I_p$ , the loop voltage, poloidal coil currents  $I_{PF}$ , the  $H\alpha$  intensity, absolute extreme ultra violet (AXUV) bolometer signal, electron density ( $n_e$ ) and temperature ( $T_e$ ), and hard X-ray (HX) count and energy, with the 230 kW 28 GHz-wave of  $N_{||} = 0.78$  at the ECR layer.

#### References:

- [1] T. I. Tsujimura, H. Idei, *et al.* Fusion Eng. and Des. **114** (2017) 97.
- [2] H. Idei, *et al.* Nucl. Fusion **57** (2017) 126045.

## 国際化推進共同研究概要

No. 2

タイトル: EC and EBW simulations in QUEST plasmas.

研究代表者: BERTELLI, Nicola

所内世話人: 出射 浩

研究概要:

電子サイクロトロン加熱による非誘導プラズマ電流立ち上げにつき、加熱・電流駆動機構を、光線追跡法、フォッカープランク準線形解析で検討した。光線追跡で加熱・吸収、プラズマ内に励起された波動電界分布を解析し、それを用いたフォッカープランク準線形解析で駆動電流を評価し、解析法の妥当性を確認した。

## EC and EBW simulations in QUEST plasmas

N. Bertelli<sup>1</sup>, R. Harvey<sup>2</sup>, and M. Ono<sup>1</sup>

<sup>1</sup>Princeton Plasma Physics Laboratory, Princeton, NJ, U.S.A.

<sup>2</sup>CompX, Del Mar, CA, U.S.A.

Numerical electron cyclotron (EC) simulations have been performed by ray tracing code GENRAY [1, 2] and the Fokker-Planck code CQL3D [3, 4] in order to better understand the QUEST fully non-inductive experiments. As for ray tracing simulations, we have assumed 20 rays to represent the EC beam and parabolic kinetic plasma profiles (see Figure 1a).

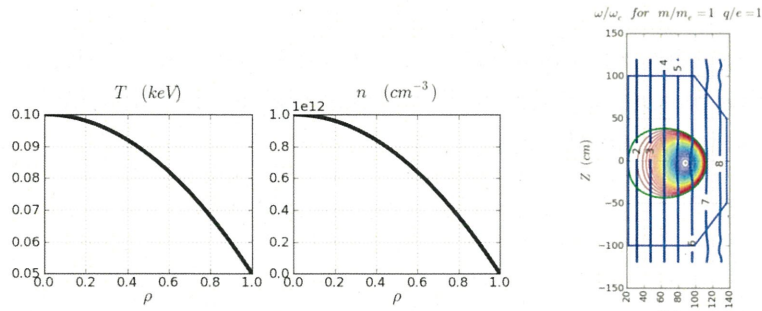


Figure 1. (a) Electron temperature and density parabolic profile; (b) magnetic equilibrium geometry.

Moreover, a cold plasma dispersion relation has been selected with an input power of 0.3 MW. Several cases have been considered changing the core and the edge values of the electron density and temperature profiles (see Table 1). Figure 2 shows a narrow power deposition profile peaked at location of the 2<sup>nd</sup> EC harmonic (i.e., in the high-field-side near the center stack) obtained by GENRAY.

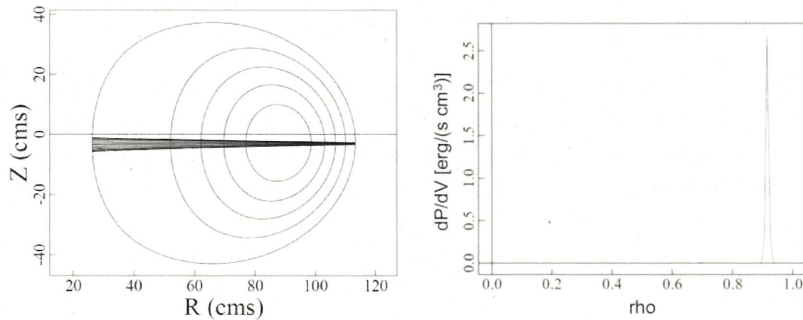


Figure 2. (a) EC ray trajectories obtained by GENRAY; (b) Power deposition profile as a function of  $\rho$ .

By making use of these GENRAY simulations we performed a series of CQL3D simulations. We have generally and preliminary obtained the following: (i) a strong non-Maxwellian tail (representing high energy electrons) in the electron distribution function at the location of the 2<sup>nd</sup> EC harmonic in the plasma (see Figure 3b); (ii) lower non-inductive total current with respect to the experimental results (see Figure 4).

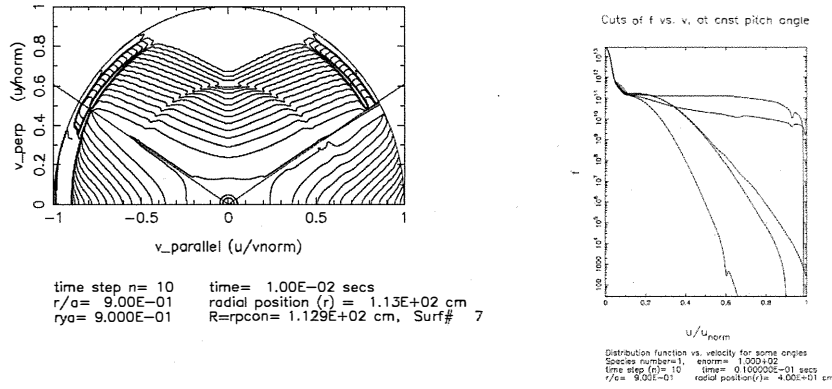


Figure 3. (a) Electron distribution function  $f(v_{\parallel}, v_{\perp})$  at  $r/a = 0.9$ ; (b) electron distribution function for a fixed pitch angle at  $r/a=0.9$ .

Regarding the latter point, additional work is necessary and still ongoing. For instance, a better representation of the plasma profiles and a different magnetic equilibrium reconstruction should be considered in the future simulations.

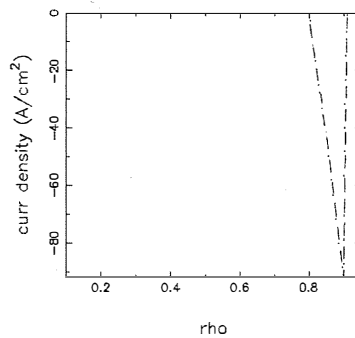


Figure 4. Electron current density evaluated by CQL3D corresponding to a total current of  $I_{cd}=34$  kA.

### Future plans

We plan to continue on this work particularly performing additional CQL3D simulations in collaboration with Prof. Hiroshi Idei. In particular, we would like to use more realistic data, different dispersion relation and magnetic field equilibrium. Finally, a comparison between the SXR data with the corresponding CQL3D synthetic diagnostic is foreseen.

### References

- [1] A. P. Smirnov and R. W. Harvey, Bull. Am. Phys. Soc. 40, 1837 (1995).
- [2] N. Bertelli et al, Phys. Plasmas 19, 082510 (2012).
- [3] Harvey W and McCoy M 1992 Proc. IAEA Technical Committee Meeting on Simulation and Modeling of Thermonuclear Plasmas p 489.
- [4] Y. Petrov and R. Harvey, Plasma Phys. Control. Fusion **58** (2016) 115001.

## 国際化推進共同研究概要

No. 3

タイトル: Measurement of edge turbulence and coherent modes and their effect on plasma confinement and transport in QUEST

研究代表者: BANERJEE, SANTANU

所内世話人: 出射 浩

研究概要: QUEST 装置で観測され Blob の発現につき、高速カメラによる観測に基づいた映像解析にて、発現、伝搬の様子を明らかにした。観測される乱流の相関解析で、揺動の伝搬を評価し、研究成果を学術論文としてまとめ、投稿した。

## Report on the international joint research for 2017-18.

Topic: Measurement of edge turbulence and coherent modes and their effect on plasma confinement and transport in QUEST

**Santanu Banerjee**  
Scientific Officer – E,  
Institute for Plasma Research,  
Bhat, Gandhinagar 382 428, Gujarat, INDIA

During the tenure of this collaborative research, intensity fluctuations recorded using the fast camera imaging technique are analyzed in the slab annular plasma as a function of magnetic shear and connection length in the spherical tokamak QUEST. Slab annular plasmas feature open magnetic field lines and can mimic the tokamak edge-SOL-like plasma attributes reasonably well. Three magnetic shear regimes are realized using three poloidal field (PF) coil pairs. A whole range of connection lengths ( $\sim \infty \geq L_c \geq 5.5$  m) is scanned by varying the PF strength for a given toroidal field for each magnetic shear regime. This for the first time a systematic study of the effect of magnetic shear and field line pitch together on edge-scrape off layer (SOL)-like plasma fluctuations is being reported. Slab plasmas with intermediate magnetic shear is observed to be more susceptible to generate distinct blobs when  $L_c$  is reduced by increasing the PF strength. A distinct coherent mode appears only at the lowest magnetic shear slab featuring a deep potential well. Such mode is not apparent at other magnetic shear cases even at the same  $L_c$ . Finally, with a combination of PF coil pairs, both the features of intermediate and low magnetic shear slabs are shown to be realizable simultaneously. Significantly stronger blobs are observed with such combination of PF mirror ratios in the presence of the coherent mode. This study may provide a better insight on the effect of magnetic configuration in tokamak edge and SOL turbulence and can help searching better tools to control cross-field convective intermittent transport in tokamaks.

### Fast visible imaging system on QUEST

The fast visible imaging system is now equipped with a new fiber bundle and modified fixtures and front end lens holder assemblies. This give more maneuverability to the optics and it is now easier setting it up. Fig. 1(a) shows the back end of the fiber bundle connected to the fast camera through the image intensifier. Also, the front end can be seen in Fig. 1(b). The front end unit enables us to rotate the fiber view in alt-azimuth directions. Fig. 2(b) shows the top view of QUEST with the field of the fast camera as the shaded region.

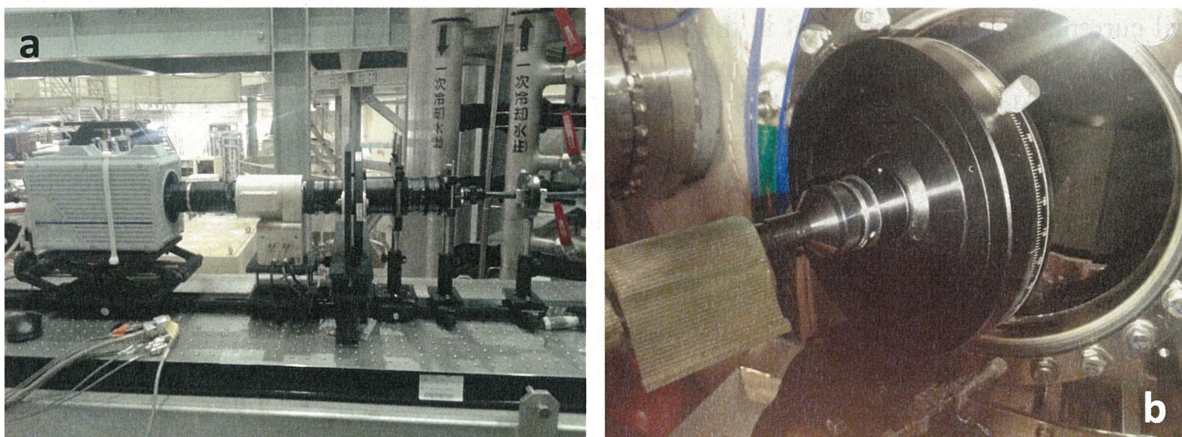


Fig. 1: (a)-(b), Back and front end of the fiber bundle on the fast visible imaging system.

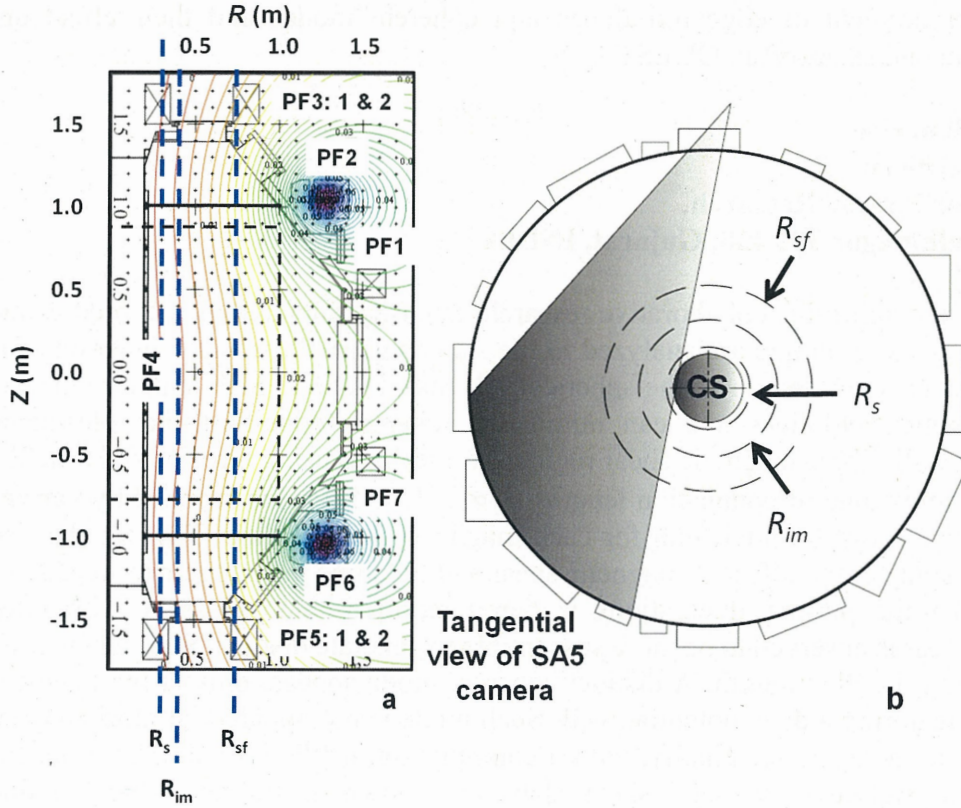


Fig. 2: (a) cross sectional view of the QUEST vessel showing the poloidal field (PF) coils and the arbitrary positions of the three regions of ‘source ( $R_s$ )’, ‘intermediate ( $R_{im}$ )’ and ‘source-free ( $R_{sf}$ )’. Magnetic field lines for the PF26 coil pair (in blue) are shown as thin lines. Black dotted rectangle shows the extent of the images and solid horizontal lines represent the divertor plates (b) top view of QUEST showing the field of the fast camera.

### Experimental detail

Slab-annular plasmas, intersecting the divertor plates, are initiated with hydrogen and using ECRH at 2.45 GHz continuous wave (CW), and pulsed with 8.2 GHz ECRH. In this pulsed phase, the 8.2 GHz ECRH driven slab plasma dominates. Plasmas extend vertically near the resonance layer  $R_{res}$  ( $\sim 0.24$  m) corresponding to the resonant field of  $B_{t_{res}} = 293$  mT, and diffuse outwards depending on RF power and  $B_z/B_t$ .  $B_z$  is varied in both curvature and strength by different poloidal field coil combinations (PF17, 26 and 35-12, as shown in Fig. 1(a)) and coil currents.  $B_t$  is kept constant in the experiment. PF strength can be quantified in terms of the pitch distance  $\Delta_z = 2\pi R B_z/B_t$ , connection length of field lines  $L_c = 2\pi R 2b/\Delta_z$  between the two divertor plates and pitch angle  $\vartheta = \tan^{-1}(B_z/B_t)$ . While referring to  $L_c$ , we always specify it at  $R=0.48$  m, which is slightly away from the source plasma and coincide with the ECR 2<sup>nd</sup> harmonic. This radial location also represents the density gradient region and has been interpreted as the blob generation location earlier.. PF curvature can be demonstrated in terms

of the magnetic shear  $S_m = \frac{R}{\vartheta} \frac{d\vartheta}{dR}$  and the mirror ratio  $\varepsilon = (B_{t_{div}}/B_{t_{mid}})$ . For  $\varepsilon$ , the field lines

starting at the second harmonic layer on the mid-plane, are traced to calculate  $B_t$  at the launching ( $B_{t_{mid}}$ ) and terminating point on the divertor ( $B_{t_{div}}$ ). Three distinct  $S_m$  regimes for three PF coil pairs ( $S_m \sim 1.05$  for PF17,  $\sim 0.85$  for PF26, and  $\sim 0.65$  for PF35-12 at ECR 2<sup>nd</sup> harmonic) are realized. These three coil pairs will be referred, henceforth in the text, as HiMS (PF17 with High  $S_m$ ), InMS (PF26 with Intermediate  $S_m$ ) and LoMS (PF35-12 with Low  $S_m$ ).

Corresponding  $\varepsilon$  are shown in Fig. 3(b), provides deep (PF35-12), shallow (PF26), and negative ( $\varepsilon < 1$  for PF17) potential wells, respectively.

## Spectral features of fluctuations

### A. Cross-correlation

Cross-correlation coefficient ( $C_{xy}$ ) is calculated among a reference pixel and for all the pixels. It is defined as:

$$C_{xy} = \frac{\sum xy - n\bar{x}\bar{y}}{\sqrt{(\sum x^2 - n\bar{x}^2)(\sum y^2 - n\bar{y}^2)}} \quad (2)$$

Where  $x$  and  $y$  are two intensity time series signals, the bar denotes ensemble average and  $n$  is the number of samples. It is the zeroth lag of the normalized covariance function. Here we will refer this quantity as  $C_{R_s}$ ,  $C_{R_{im}}$  and  $C_{R_{sf}}$ , where the subscript stands for the radial location of the reference pixel at  $Z=0.2$  m. Thus,  $C_{R_s}$  stands for the correlation coefficient matrix for the reference pixel at  $R_s$  and  $Z=0.2$  m with all the other pixels. Fig. 3 shows the  $C_{R_s}$  and  $C_{R_{im}}$  for all the three  $S_m$  values for  $L_c \sim 14$  m. The background image represents  $C_{R_s}$ , while the overlaid contours represent  $C_{R_{im}}$ .

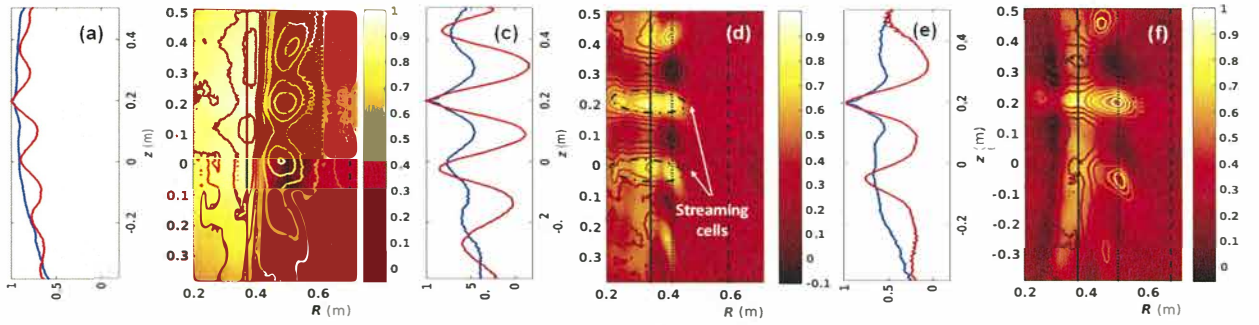


Fig. 3: Cross-correlation coefficient ( $C_{xy}$ ) is shown for (b) HiMS, (d) InMS and (f) LoMS respectively. The background image is  $C_{xy}$  with the reference pixel at  $R_s$  and the overlaid contour is the same with the reference pixel at  $R_{im}$ . Vertical lines from left show the positions of  $R_s$ ,  $R_{im}$  and  $R_{sf}$  respectively; (a), (c) and (e) show the  $C_{R_s}$  at  $R_s$  (blue) and  $C_{R_{im}}$  at  $R_{im}$  (red) respectively.

Correlation between  $R_s$  and  $R_{im}$  is smallest for the highest  $S_m$  value and intermediate for the least  $S_m$  value, while maximizing for the intermediate  $S_m$  (InMS). The connection between  $R_s$  and  $R_{im}$  is quite prominent for InMS, showing up like well-connected streaming cells, shown with broken elliptic eye-guides in Fig. 3 (d), in the cross-correlation coefficient image. For LoMS, these cells are still forming up, while for HiMS, such connections are not at all apparent at similar  $L_c$ . This strong connection between  $R_s$  and  $R_{im}$  is the most plausible reason for formation of detached blobs with InMS. As it has been seen later, InMS slabs are most susceptible to blob formation and ejection, while LoMS slabs are likely to generate detached blobs at a slightly lower value of  $L_c$  as compared to InMS. On the contrary, HiMS slabs, featuring highest  $S_m$  and  $\varepsilon < 1$ . A distinct spatial mode can be seen at  $R_{im}$  in all the three cases. Wavelength ( $\lambda_z$ ) along  $Z$  for this mode grows with decreasing  $S_m$  for similar  $L_c$ , as the PF coils are changed. Longest  $\lambda_z$  ( $= 0.3$  m) was observed for the least  $S_m$  (LoMS).

### B. Fourier analysis

Fig. 4 shows the spectrograms for intensity fluctuations at  $R_s$  (a) and  $R_{im}$  (b) respectively for LoMS at  $L_c = 14.5$  m. At  $R_s$ , this mode appears at  $\sim 3.5$  kHz and then gets downshifted slightly to  $\sim 2.5$  kHz at  $R_{im}$ . It has been seen that the mode has two radially localized lobes, one strong lobe at  $\sim 2$  cm around  $R_{im}$  and the other relatively weaker lobe at  $\sim 10$  cm inside  $R_{im}$ . Further, this mode has a long poloidal span of  $\sim 40$  cm.

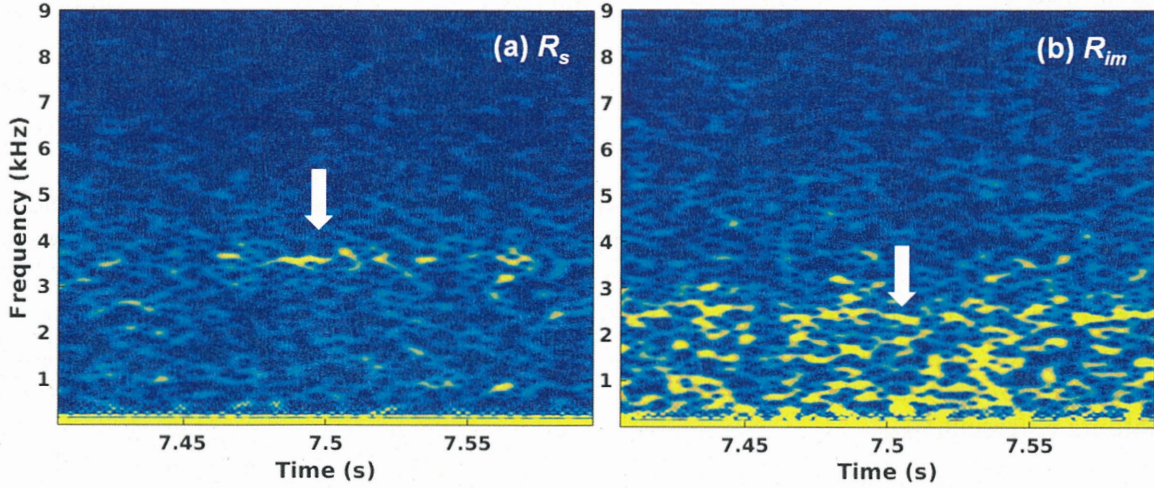


Fig. 4: (a)-(b): spectrograms for 200 ms at  $R_s$  and  $R_{im}$  respectively; The coherent mode at 3.5 kHz and 2.5 kHz at  $R_s$  and  $R_{im}$  respectively is shown by white arrows.

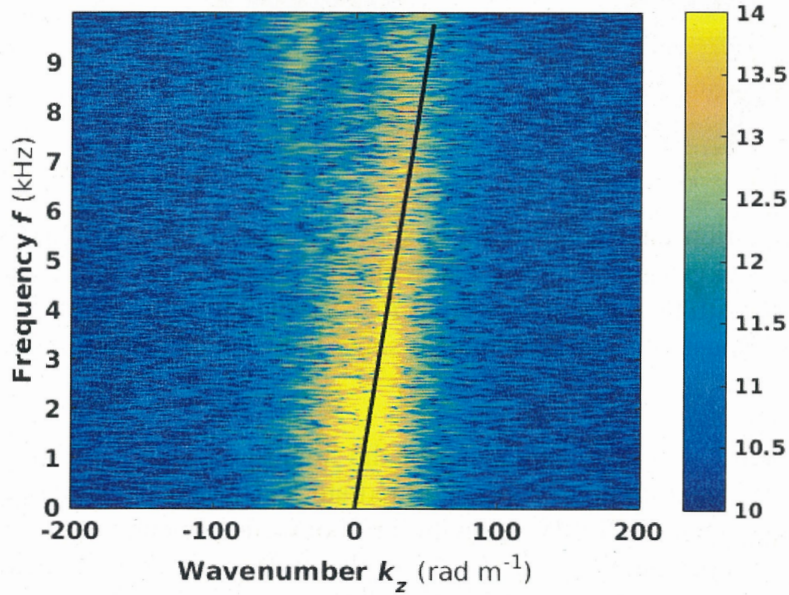


Fig. 5: InMS with  $L_c=5.9$  m; Turbulence characteristics at  $R_{im}$  in poloidal wavenumber and frequency ( $k_z$ - $f$ ) space.  $k_z > 0$  corresponds to propagation vertically up, in the IDD. Black solid line represents the linear fit.

### C. Wavenumber frequency ( $k_z$ - $f$ ) spectra

A two-dimensional discrete Fourier transform (DFT) estimate of the poloidal wavenumber-frequency ( $k_z$ - $f$ ) spectra for intensity fluctuations at  $R_{im}$  is shown for  $L_c = 5.9$  m in InMS in Fig. 5. The colorbar denotes the magnitude of DFT. All along the radial direction  $k_z$ - $f$  spectra shows a single lobe with  $k_z > 0$  fluctuations, which means fluctuation (both broadband and the coherent

mode) propagation is vertically upward in the ion diamagnetic drift direction (IDD). The measured  $k_z$ - $f$  spectra can be fitted by a single linear dispersion relation ( $f = v(k)k / 2\pi$ ) up to moderate range of frequencies such that poloidal  $v_{ph} = v_g$  for a broad range, as shown in Fig. 5. The black solid line represents the linear fit and hence poloidal phase velocity  $v_{ph}$  can be calculated. For the representative case with InMS and  $L_c=5.9$  m,  $v_{ph}$  at  $R_{im}$  is  $1.1 \text{ km s}^{-1}$ .  $v_{ph}$  stays in the range of  $1 \pm 0.1 \text{ km s}^{-1}$  for the  $L_c$  variation considered in this experiment. However, for LoMS,  $v_{ph}$  is  $0.5 \pm 0.1 \text{ km s}^{-1}$ .

### Summary of the analysis done

Fluctuation characteristics are observed to differ considerably with the variation in magnetic shear ( $S_m$ ). Slab plasmas with intermediate magnetic shear (InMS) are more susceptible to generate blobs with decreasing connection length ( $L_c$ ). Slabs with low magnetic shear (LoMS) feature triggering of a coherent mode at  $\sim 3$  kHz as  $L_c$  is decreased below  $\sim 18$  m. Slabs with high magnetic shear (HiMS) are the most stable and are not likely to generate blobs or coherent modes even at similar  $L_c$  as that of their other  $S_m$  counterparts. At InMS, fluctuations are dominated by broadband turbulence while, at LoMS, drift wave predominance is observed. Propagation direction of fluctuations remains in the ion diamagnetic drift direction (IDD) similar to tokamak SOL. Propagation velocity is double in case of InMS as compared to LoMS. Finally, when the PF coil pairs for InMS and LoMS cases are combined, considerably stronger blobs with similar average blob frequency are observed in the presence of the coherent mode. Hence, such suitable combination of magnetic shear can be used as a tool to modify the density gradient scale length at the edge, edge turbulence characteristics and thereby control the cross-field convective intermittent transport across the LCFS in tokamaks.

### Acknowledgements

I gratefully acknowledge the support of my collaborator Prof. H. Idei and PhD supervisor Prof. H. Zushi. I also acknowledge the help and support offered by my collaborator Dr. T. Onchi, and all other AFRC staff during the tenure of this collaborative effort. This work was supported by the International Joint Research Program of the Research Institute for Applied Mechanics (RIAM), Kyushu University, JAPAN.

### Publications and presentations regarding this collaboration during 2017-18.

#### Publications:

1. **Santanu Banerjee**, H. Zushi, N. Nishino, K. Hanada, H. Idei, K. Nakamura, M. Hasegawa, A. Fujisawa, Y. Nagashima, K. Mishra, S. Tashima, T. Onchi, A. Kuzmin, and K. Matsuoka, “*Effect of magnetic shear on edge turbulence in SOL-like open field line configuration in QUEST*”, submitted to Plasma Phys. Control. Fusion, 2017.

## 国際化推進共同研究概要

No. 4

タイトル: Joint study of long pulse high beta discharges and related edge turbulence transport in steady state operation (SSO) plasmas on QUEST and EAST

研究代表者: GAO, Xiang

所内世話人: 花田 和明

概要:

# RESEARCH REPORT

Date: Feb. 23, 2018

Visiting scientists: (name) Xiang Gao  
(position) Professor  
(university / institute) Institute of Plasma Physics,  
Chinese Academy of Sciences

Host scientist: (name) Kazuaki Hanada  
(position) Professor  
(university / institute) Kyushu University

Research period: (from) Jan. 25, 2018 (to) Jan.31, 2018

Research subject: **Joint study of long pulse high beta discharges and related edge turbulence transport in steady state operation (SSO) plasmas on QUEST and EAST**

## Introduction

Steady state operation (SSO) of tokamak plasma is one of the basic requirements for future fusion reactors. Long pulse high beta operation is one of important missions for ITER. Joint study long pulse high beta discharges in SSO plasma research field on QUEST and EAST is strongly supporting ITER experiment from both experience and theory. In

addition, turbulence driven transport plays an important role in long pulse high beta plasma with SSO. In QUEST and EAST, different filaments had been observed in long pulse discharges. So joint study of transport on QUEST and EAST will provide some key understandings for SSO. And also, there are many other correlated branches of long pulse high beta SSO on QUEST and EAST, exploration study on new effective diagnostics and related confinement and transport issues with SSO is also meaningful.

### **New published experimental results on QUEST and EAST in 2017**

On QUEST, Fully non-inductive plasma maintenance was achieved by a microwave of 8.2 GHz and 40kW for more than 1 h 55 min with a well-controlled plasma-facing wall (PFW) temperature of 393 K, using a hot wall and a limit configuration, as shown in Fig.1. [K.Hanada et al., NF2017].

The PFW was composed of atmospheric plasma-sprayed tungsten and stainless steel. The hot wall plays an essential role in reducing the amount of wall-stored hydrogen and facilitates hydrogen recycling. The longest duration of plasma maintenance was 1 h 55 min, during which the predicted particle balance was partially confirmed. For similar plasma parameters, such as the plasma current, density and  $I_{H\alpha}$ , which are expected to deposit an equivalent H flux on the PFW, the wall pumping rate and global recycling ratio at the same amount of wall-stored H strongly depends on the wall temperature. A fuel particle balance equation based on the presence of a hydrogen transport barrier between the deposited layer and the substrate was applied to the long-duration discharges. It was found that the model could readily predict the observed behaviour in which a higher wall temperature likely gives rise to faster wall saturation. The experimental data indicates that regulation of the wall temperature will make it possible to avoid the uncontrollability of density in the SSO. When the uncontrollability of density arises, tentative reduction of the wall temperature can enhance wall pumping and is the way to produce a recovery. After recovery, the wall temperature should be returned to the standard high temperature. This is another use of the hot wall for SSO.

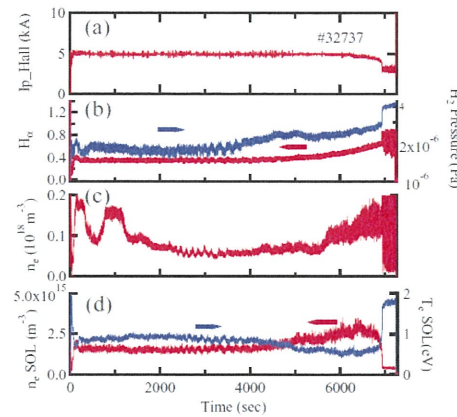


Figure 1 1h55min long pulse discharge on QUEST(K.Hanada et al., NF2017).

On EAST, high beta<sub>N</sub> (~1.8) plasma with good confinement (H98y2~1.1) on EAST tokamak has been reported [X.Gao et al., NF2017]. These ELMy H-mode plasmas with B<sub>t</sub>=1.6T, I<sub>p</sub>=400 kA and q<sub>95</sub>≈4.5 were heated by lower hybrid wave and neutral beam injection. The internal transport barrier (ITB) and edge transport barrier (ETB) are both observed with m/n=1/1 fishbone, which were identified to clamp central q at values close to unity. Implying an improved H-mode with flat central q profile and absence of sawteeth, like other devices. ITB dynamics, stable high heating power and control of impurity radiation could be considered as the key to achieving long-pulse high-β<sub>N</sub> operation with EAST.

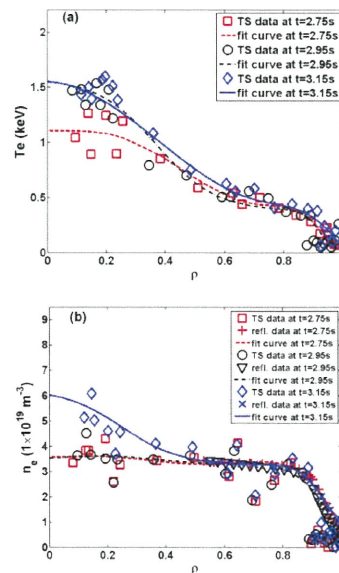
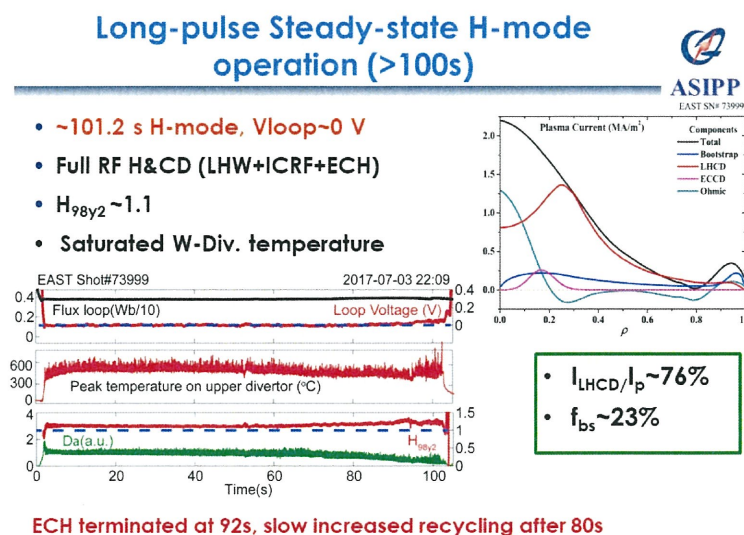


Figure 2 High beta<sub>N</sub> long pulse discharges with ITB+ETB (X. Gao et al., NF2017).

And also recent experiments on EAST have achieved the 101.2s H-mode with zero loop voltage and an ITER-like tungsten divertor, base on the optimized current profile, better confinement ( $H_{98y2} \sim 1.1$ ) with an electron ITB was obtained, also with flat central q profile and absence of sawteeth at high betaP regime with  $B_t=2.5T$ ,  $I_p=400$  kA[H.Q.LIU,et al.,ITC26&APFA2017]. These improved H mode discharges with optimized flat central q profile can be as good candidate for long pulse operation scenarios for ITER. These experiments also strengthen the physics basis for achieving high performance, steady state discharges in future burning plasmas.



13

Figure 3 101.2 s long-pulse SSO H-mode operation on EAST [H.Q.LIU,et al.,ITC26&APFA2017]

## Discussions

QUEST and EAST are both to develop the scientific basis for achieving a steady state condition. Now here has a new start point for the comparative and joint study on QUEST and EAST, especially in high beta discharges, high performance SSO operation. The joint study results now and in future may shed light on the ITER SSO scenario.

During this visit, several interesting topics are also involved in discussions. Those are “2D-SXR imaging system on QUEST” and “Probe system in CHI” by Mr. C.B.Huang, “Study on the thickness profile of deposited film forming on the plasma-facing wall in the QUEST tokamak” by Mr. Z.X.Wang, “Progress of calorimetric measurement of heat load in

EAST” by Mr. Y.K.Liu. Based on the fruitful communications, the abundant progress and requirement of future research of this project are expected and deeply joint research is required in future.

### **Acknowledgement and comments:**

Work supported by the international joint research at the Joint Usage of Research Centers for Applied Mechanics for 2017. We would like to thank our host, Professor K. Hanada, who helps a lot during our staying at QUEST and very appreciate the useful discussions and comments. It is a good chance for us to join in study in the QUEST. Also QUEST staffs and students are thanked for their helpful discussions. Ms. Masuike is thanked for her kindly helps for this visit. We hope that the international joint research at the Joint Usage of Research Centers for Applied Mechanics could continue to enhance China-Japan cooperation on fusion plasma research in the future.

### **Co-Publications in 2017:**

[1] X. Gao,..., H.Q.Liu,...,K. Hanada, et al., Nucl. Fusion 57 (2017) 056021.

[2] Y. K. Liu, N. Hamada, K.Hanada, X.Gao, H.Q.Liu,..., J.P.Qian, et al., Plasma Phys Control Fusion 59(2017) 045009.

(Signature)\_\_\_\_\_

(Name in print) Xiang Gao\_\_\_\_\_

## 国際化推進共同研究概要

No. 5

タイトル: Joint study of calorimetric measurement of heat load and power balance estimation in steady state operation (SSO) plasmas on QUEST and EAST

研究代表者: LIU, Haiqing

所内世話人: 花田 和明

研究概要:

## RESEARCH REPORT

Date: Feb. 23, 2018

Visiting scientists: (name) Haiqing LIU

(position) Associate Professor

(university / institute) Institute of Plasma Physics,  
Chinese Academy of Sciences

(name) Yinxian Jie

(position) Professor

(university / institute) Institute of Plasma Physics,  
Chinese Academy of Sciences

Host scientist: (name) Kazuaki Hanada

(position) Professor

(university / institute) Kyushu University

Research period: (from) Jan. 25, 2018 (to) Jan.31, 2018

Research subject: Joint study of calorimetric measurement of heat load and power balance estimation in steady state operation (SSO) plasmas on QUEST and EAST

## Introduction

Steady state operation (SSO) of magnetic fusion devices is one of the goals for fusion research. As it is predicted that an enormous heat flux ( $10\text{MW}/\text{m}^2$ ) is coming to the diverter (vertical heat target) locally from the plasma in the future fusion reactor, the heat load distribution (power balance) and its control should be investigated to realize future fusion power plants. Actually, control of contact point of PFCs to plasma has been applied in many long duration discharge devices such as TRIAM-1M, QUEST, EAST and on which long duration discharges can be successfully obtained. However, the longest plasma is spontaneously terminated and the reason is still unclear. Plasma confinement degeneration during long-pulse discharge could be caused by increment of first wall temperature then boundary recycle enhance. So water cooling of PFCs is important to achieve high parameter and long-pulse operation in EAST. The cooling capability strongly depends on the distribution of the heat load to the PFCs, the change of distribution of the heat load strong depends on plasma confinement. Understanding of plasma parameters dependent on distribution of the heat load is in favor of extrapolating result to ITER. It's certainly worth researching distribution of heat load of PFCs in EAST with steady-state or long-pulse operation. Injected power should be equilibrium with heat load brought by cooling water system. Measurement of heat load and researching of power balance in EAST and QUEST will provide crucial support for ITER experiments. On QUEST, a fully non-inductive plasma was achieved more than 1 h 55 min with a well-controlled plasma-facing wall (PFW) temperature of 393 K, using a hot wall and a limit configuration, Although the strong modification of plasma configuration was applied in QUEST, much of the heat load to the outer vessel was still remained. It means that the heat load is mainly supplied from energetic electrons which are generated by injected RF electric field. EAST device have fully actively water cooled plasma facing components (PFCs), so calorimetric measurement can be easily applied to measure heat load of PFCs on EAST. In 2017, 101.2 s long pulse H mode plasma was obtained. We can derive the heat load distribution and power balance during steady - state operation. Joint study of calorimetric measurement of heat load and power balance estimation in steady state operation (SSO) plasmas on QUEST and EAST will give heat load and power balance database for SSO plasma.

### Recent experimental progress on QUEST and EAST

On QUEST, the calorimetric measurement had done of direct loss of energetic electrons on QUEST, as shown in Fig. 1.. Two movable water-cooled limiters made of W were installed to effectively remove the heat load from the energetic electrons. Total heat load on MLs located in LFS is corresponding to 10% (5kW) of the inject RF power (50kW) and approximately constant, selectively heat flows into MLs that is locally protruding plasma side. Additionally, heat load of the MLs is due to the plasma which is strongly dependent on the magnetic field lines structure. Heat load on MLs is not due to the bulk plasma as a result from that the distance between the position of outermost magnetic surface and MLs, greatly accelerated energetic electrons at the resonant layer by RF injected hits the MLs directly. On QUEST, Fully non-inductive plasma maintenance was achieved by a microwave of 8.2 GHz and 40kW for more than 1 h 55 min with a well-controlled plasma-facing wall (PFW) temperature of 393 K, using a hot wall and a limit configuration [K.Hanada et al., NF2017]. However, active cooling does not work at present because of the lack of a connection to the water-cooling channel. Because the hot wall is always exposed to the heat load from the plasma, such as that from the charge exchange neutrals and escaping plasma as well as radiation during plasma discharges, the surface temperature of the hot wall rose by approximately  $30\text{ }^\circ\text{C}$  during 1 h 55 min of discharge. The PFWs in the mid-plane areas are composed of thin stainless steel panels and their temperature is likely to rise during discharge,

even though they are not actively heated. During the longest discharge, the temperature of the PFW in the mid-plane area rose from 373 K to 473 K.

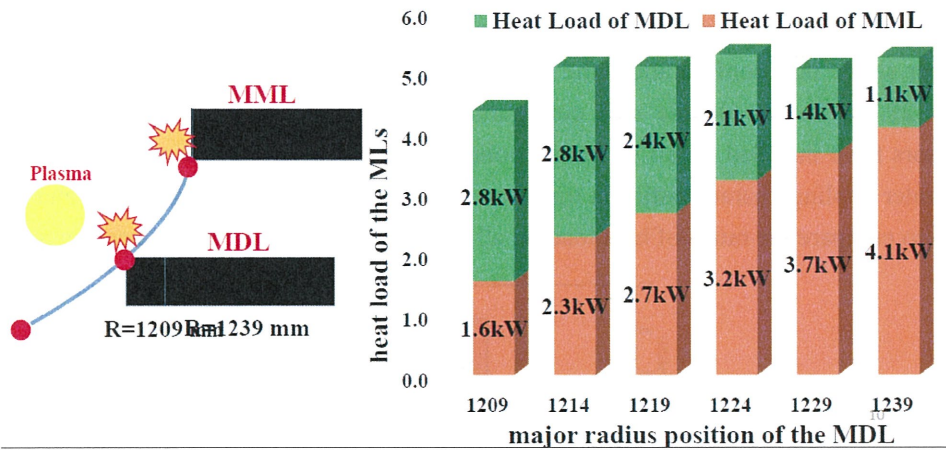


Figure 1 Long pulse or SSO plasma (Mr. Hamada's presentation when he visited in ASIPP).

On EAST, it is impossible to derive an absolute quantity of heat load result from the wall temperature, so it is most important to inquire the Water-Cooling System( control system of the flow rate and water temperature) The EAST tokamak has also been equipped with a pressurized water system to cool all the PFCs to allow long pulse and high injected energy discharges to be achieved. EAST's water-cooling system consists of five main water cooling modules. In the 2015–2016 campaign, sensors are only installed on the D module, namely the strike point region on the lower divertor target, the heat load on this region was measured using the cooling water calorimetry diagnostic[ Y.K.Liu et al, PPCF2017].

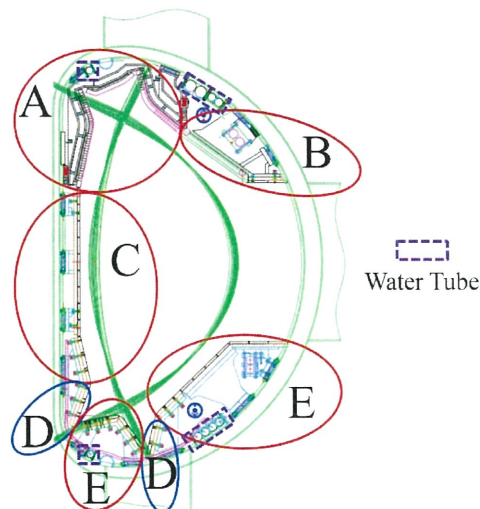


Figure 2. Schematic diagram of water cooling modules on EAST presented from poloidal cross-section. A is integral upper divertor; B is upper passive plate and upper low field side; C is non-strike point region on lower inner divertor, high field side; D is strike point region on lower divertor; E is lower dome, non-strike point region on lower outer divertor, lower passive plate and lower field side. [Y.K.Liu, PPCF2017]

Typically, double null configuration and upper or lower single null configurations in EAST can be produced and stably controlled. The ratios of heat load on D module to total injected energy including ohmic energy and auxiliary heating energy with three kinds of plasma configurations are shown in Figure 3. In upper single null configuration, the heat load on D module is only 4.9% of total injected energy. And it's 21.7% for the double null configuration. In 2017 experiments, flow meters and temperature sensors have installed on all of water cooling modules (A-E) instead of only D module to investigate the water cooling characteristics in upper and lower divertor made by tungsten and graphite respectively, and to compare the ratios of heat load on all of modules with three plasma configurations.

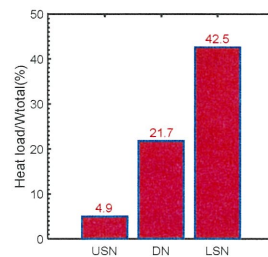


Figure 3. The ratio of heat load on D module to total injected energy including ohmic energy and auxiliary heating energy with upper single null(USN), double null(DN) and lower single null (LSN) plasma configuration, respective. [Y.K.Liu, PPCF2017]

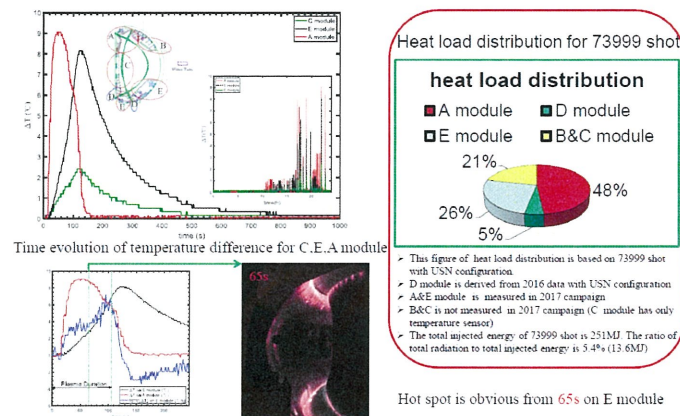


Figure 4. In 2017, a calorimetric measurement of heat load on A and E module was carried out during 101.2s long-pulse H-mode discharges in EAST. [Y.K.Liu's presentation during this visit]

A calorimetric measurement of heat load on A and E module was carried out during 101.2s long-pulse H-mode discharges in EAST, as shown in Fig.4. The measurement on C and D module is incomplete. B module is no temperature sensor and flow meter. The saturation of water temperature difference in upper divertor during long-pulse discharge realized. However, the saturation in lower divertor not realized. The thermal time constant are 105.3 and 12.3 respectively. Considering the energy balance of the EAST long-pulse discharges with the USN configuration, the output energy detected by the cooling water calorimetry diagnostic on the D module amounted to 45.5%. This value is colsed to 42.5%, which is the ratio of heat load on D module to total injected energy in LSN configuration. In the USN configuration, the parameter of Drsep is larger, the possibility that hot spot comes out on dome of lower divertor is smaller. The influence of energetic electron on the dome of lower divertor is not clear.

## Discussions

Because measurement of heat load and researching of power balance in EAST and QUEST will provide crucial support for ITER experiments. This subproject was continued to be supported by the National Magnetic Confinement Fusion Program of China with Contract No. 2014GB106002 (Associate Prof. Liu) in the next years. The joint study of QUEST and EAST will push this subproject forward in the next year.

During this visit, several interesting topics are also involved in discussions. Those are “2D-SXR imaging system on QUEST” and “Probe system in CHI” by Mr. C.B.Huang, “Study on the thickness profile of deposited film forming on the plasma-facing wall in the QUEST tokamak” by Mr. Z.X.Wang, “Progress of calorimetric measurement of heat load in EAST” by Mr. Y.K.Liu. Based on the fruitful communications, the abundant progress and requirement of future research of this project are expected and deeply joint research is required in future.

## Acknowledgement and comments:

Work supported by the international joint research at the Joint Usage of Research Centers for Applied Mechanics for 2017. We would like to thank our host, Professor K. Hanada, who helps a lot during our staying at QUEST and very appreciate the useful discussions and comments. It is a good chance for us to join in study in the QUEST. Also QUEST staffs and students are thanked for their helpful discussions. Ms. Masuike is thanked for her kindly helps for this visit. We hope that the international joint research at the Joint Usage of Research Centers for Applied Mechanics could continue to enhance China-Japan cooperation on fusion plasma research in the future.

## Co-Publications in 2017:

- [1] X. Gao, ..., H.Q.Liu, ..., K. Hanada, et al., Nucl. Fusion 57 (2017) 056021.
- [2] Y. K. Liu, N. Hamada, K.Hanada, X.Gao, H.Q.Liu, ..., J.P.Qian, et al., Plasma Phys Control Fusion 59(2017) 045009.

## Publications which had acknowledged to “the Collaborative Research Program of the Research Institute for Applied Mechanics, Kyushu University” in 2017:

- [1] Y. K. Liu, N. Hamada, K.Hanada, X.Gao, H.Q.Liu, ..., J.P.Qian, et al., Plasma Phys Control Fusion 59(2017) 045009.
- [2] G. Li, ..., H.Q.Liu, et al., Plasma Sci Technol. 19(2017) 084003.
- [3] H.Lian, H.Q.Liu, et al., Journal of instrumentation, 12(2017)C12036.
- [4] Z.Y.Zou, H.Q.Liu, et al., Review of scientific instruments, 89 (2018) 013510.

(Signature) \_\_\_\_\_

(Name in print) Haiqing Liu, Yinxian Jie

## 国際化推進共同研究概要

No. 6

タイトル: Theory on nonlinear dynamics of trapped electron turbulence.

研究代表者: HAHM, T, S

所内世話人: 小菅佑輔

概要: 近年の運動論的数値実験の進展から、捕捉電子乱流においても階段状分布が現れることが報告されている。

本研究では、この捕捉電子乱流における階段状分布について理論モデル導出を目指している。そのために研究打ち合わせを行い、一つの方策としてイオン温度階段状分布形成モデルの捕捉電子乱流への拡張に取り組むことを決定した。

今年度の初期的な解析から、断熱電子に対して導出されていた交通渋滞モデルの非断熱電子を含む場合に拡張する見通しを得ることができた。

# Theory on nonlinear dynamics of trapped electron turbulence

Seoul National University

T.S. Hahm

## Introduction:

Developing a predictive model for turbulent transport is a critical issue for the research on plasma turbulence and fusion energy. While quasilinear models are widely used, there are several researches that report the failure of this approach. In particular, the validity of quasilinear transport models is often violated for typical plasma turbulence, which has the Kubo number of order unity. Indeed, recent gyrokinetic simulation reports that trapped electron turbulence has the Kubo number of order unity or more[1]. Moreover, formation of corrugated temperature profile in nonlinear gyrokinetic simulation is also reported[2]. It is a critical issue to develop a model beyond quasilinear theory for predicting electron energy and particle transport driven by TEM. In this work, we aim at initiating a research toward understanding nonlinear and non-local dynamics of TEM turbulence.

## Results:

An approach for staircase formation is based on traffic jam model[3]. In this approach, a key idea is to introduce the time delay between instantaneous heat flux and the mean heat flux. The time delay is analogue of driver's response time in traffic jam model. When the response time is long, traffic jam formation is expected. In the terminology of plasma turbulence, the time delay arises from the nonlinear ExB mixing. Due to the nonlinear ExB mixing, the heat flux relaxes towards the mean diffusive flux, while the instantaneous heat flux can deviate from the mean. The time evolution for heat flux is derived for simplified ITG turbulence model in the previous study[3].

In order to extend the previous result, we analyzed the time evolution of heat flux for different models of turbulence. In this study, we start with slab-ITG from 1D drift kinetic equation. In this case, the time evolution of the two point correlation function of phase space density fluctuation[4,5] is given by

$$\partial_t \langle \delta f(1) \delta f(2) \rangle + T(1,2) = P(1,2),$$

$$T(1,2) = \tau_c^{-1} \ln F(\vec{x}_-, \vec{v}_-) \langle \delta f(1) \delta f(2) \rangle,$$

where  $\delta f$  is the fluctuating part of distribution function,  $P(1,2)$  is the production term with free energy release,  $\tau_c^{-1}$  is the inverse of ExB mixing time (correlation time), and  $F(\vec{x}_-, \vec{v}_-)$  is the function of the difference of space and velocity. Specific form of the factor differs for the models of turbulence. The case of slab-ITG with 1D drift kinetic equation is given in [5].

The evolution of heat flux is obtained by averaging over the velocity space:

$$\partial_t Q = -\bar{\tau}_{mix}^{-1} (Q - Q_0),$$

$$\bar{\tau}_{mix}^{-1} = v_{th}^{-1} \int_{-\Delta v}^{\Delta v} dv \tau_c^{-1} \ln F(\vec{x}_-, \vec{v}_-).$$

The integration can be performed analytically and the inverse of the mixing time typically scales with the ion transit time  $k_{\parallel} v_{th}$ . We note that the procedure can be applied to TEM turbulence as well[4]. In this case, in addition to the form factor, we also need to consider the effect of non-adiabatic electrons, which can appear as additional contribution in the heat flux evolution equation. More detailed analysis, as well as implications on the formation of corrugated profiles, is currently on-going and will be reported in future.

## References

1. Y. Xiao and Z. Lin, Phys. Rev. Lett. **103** (2009) 085004
2. Lei Qi, et al., Nucl. Fusion **57** 124002 (2017)
3. Y. Kosuga, et al., Phys. Rev. Lett. **110** 105002 (2013)
4. G.J. Choi and T.S. Hahm Phys. Plasmas **23** (2016) 072301
5. Y. Kosuga, et al., Nucl. Fusion **57** 072006 (2017)

## Research members

T.S. Hahm (SNU), Y. Kosuga (Kyushu Univ.), G.J. Choi (SNU), K. Hasamada (Kyushu Univ.), F. Kin (Kyushu Univ.)

## 国際化推進共同研究概要

No.7

タイトル: Investigation of rotation reversal near resonance layer in an EC heated/driven plasma.

研究代表者: MISHRA, KISHORE, KANTI

所内世話人: 出射 浩

概要: 電子サイクロトロン加熱では、プラズマに直接的に運動量を付加しない加熱法であるが、近年、電子サイクロトロン加熱によって生成されたトカマクプラズマで、自発的なプラズマの回転が報告されている。QUEST 装置でもドップラー分光で、自発的なプラズマの回転が観測された。回転には高速電子生成・損失過程が関連していることが理論的に検討されている。高速電子生成には、加熱・吸収効果を適切に扱う必要があり、入射偏波面の検討を進めた。

# A short report on, “Study of EC induced intrinsic rotation in QUEST tokamak”

By Kishore Mishra

Institute for Plasma Research, Gandhinagar, India, 382 428

## Background and Motivation:

Plasma rotation stabilizes magneto hydro dynamics (MHD) instabilities. Torque to rotate plasma in toroidal direction can be given externally by neutral beam injection or resonant magnetic perturbation. However, at high beam energy and density like the conditions to be prevailed in ITER or DEMO reactors, externally momentum driven rotation may not be significant. Spontaneous rotation with radio frequency (RF) heating on the other hand has been observed in many tokamaks and is intrinsic in nature without any external torque injection. The mechanism of the RF induced intrinsic rotation and the ways to control it has not been understood adequately. Therefore, mechanism of spontaneous rotation after RF heating is an important topic to understand.

In QUEST spherical tokamak, plasma current is non-inductively started up and driven by Electron Cyclotron Waves (ECW). Spontaneous rotation of such ECW driven plasma has been observed with the help of Doppler spectroscopy and Mach probe measurements. Recent experiment with 28 GHz-ECW shows that plasma current  $I_p > 80$  kA, could be driven with ECWs alone. Local heating is enhanced using two quasi-optical mirrors, where the beam waist at resonance is about 5 cm in diameter. For instance, the power density around EC resonant layer reaches  $5 \text{ MW/m}^2$  at 150 kW incident power.

In addition, the polarizer for incident EC wave has been installed. It consists of two phase shifters ( $\lambda/4$  and  $\lambda/8$ ), where  $\lambda$  is a wavelength of 28 GHz EC wave. Incident wave polarization can be adjusted to select O- and X-modes by turning the plates around and changing the polarizer angles. In the QUEST plasma experiment, dependence of plasma current on

the polarizer angles has been observed. Relationship between the  $\lambda/8$  plate and plasma current is presented in Fig. 1. As current start-up failed at the angle around 1.0 radian; attained plasma current depends on angle of the  $\lambda/8$  plate. According to such tendency, it is clear that plasma response depends on polarization of incident wave. Spontaneous rotation can be changed by condition of the current drive. Therefore, fine polarization control is required to understand the mechanism how incident EC-wave generates spontaneous rotation. Unfortunately, relationship between the plate-angle combination and the polarization had not been well surveyed when the dependence shown in Fig.1 was investigated.

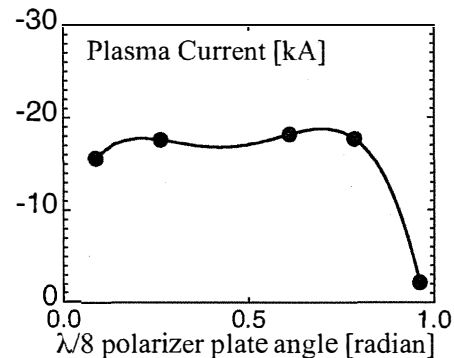


Fig.1: Non-inductively ramped plasma current, depending on one-eighth  $\lambda$  polarizer-plate angles

### Experimental Method:

Polarizer assembly consisting of  $\lambda/4$  and  $\lambda/8$  phase shifter plates were tested using a low power 28 GHz RF source. The transmitted HE11 mode was generated by a mode converter. Angle of each plate can be turned around and adjusted with accuracy of 0.1 degree. In this test, we set 100 angle settings (10 for each plate) and measured horizontal and vertical electric fields,  $E_x$  and  $E_y$ . As shown in Fig.2, in the

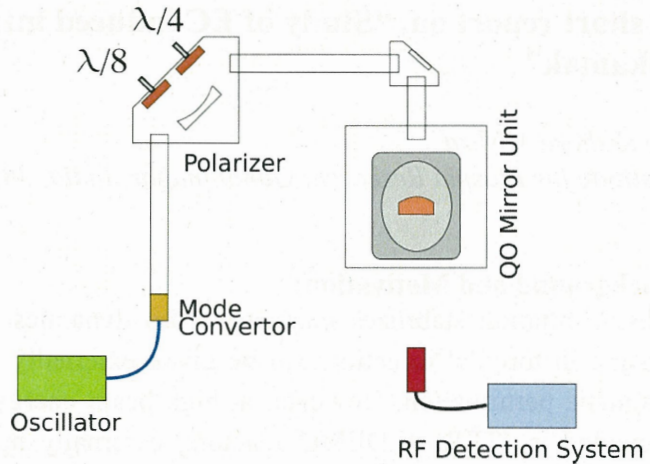


Fig. 2: Experimental setup of the low power test to investigate polarization of 28 GHz EC wave.

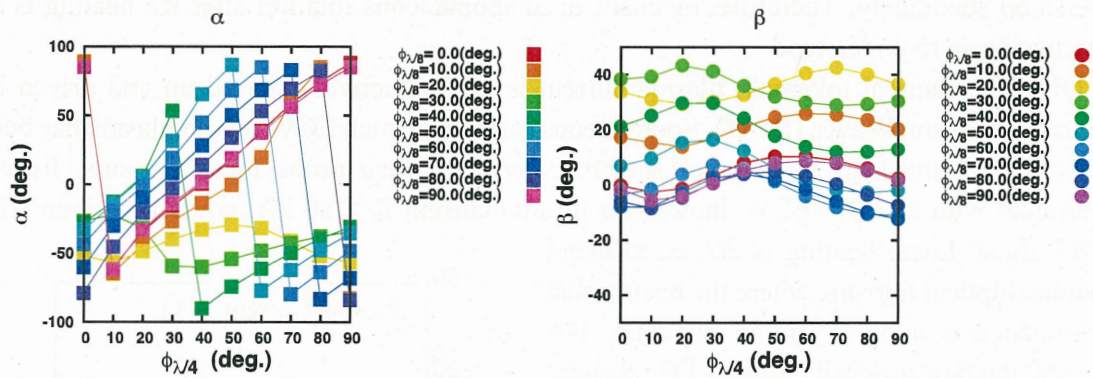


Fig. 3:  $\alpha$  and  $\beta$  dependences on the plate angles, evaluated from the  $E_x$  and  $E_y$  measurement. Here  $\alpha$  is the angle from long axis of polarization ellipse and  $\beta$  is its elongation. The horizontal axis is the angle of the  $\phi_{\lambda/4}$  plate.

experimental set-up, 28 GHz wave (0.01 W) of the HE11 mode passes through a polarization unit, a miter bend, and the two quasi-optical (QO) mirrors. Assuming actual EC wave injection in QUEST, the detector was installed around the EC resonance layer position of 28 GHz EC wave.

Figure 3 shows  $\alpha$  and  $\beta$  dependences on the plate angles, evaluated from the  $E_x$  and  $E_y$  measurement. Here  $\alpha$  is the angle from long axis of polarization ellipse and  $\beta$  is its elongation. The wide  $\alpha$ - $\beta$  ranges of the ellipse polarization states were properly controlled, depending on the plate angles. Careful verification of the polarization setting at the current-drive experiment is required. The evaluated polarization states are going to be compared with those calculated from the numerical code. Future work on this topic is to measure intrinsic rotation profiles during EC injection at different polarizer settings.

### Acknowledgements:

This research is carried out under international joint research grant from Research Institute for Applied Mechanics, Kyushu University. The author gratefully acknowledges active support and guidance of RIAM collaborators Prof Hiroshi Idei, Prof. Hideki Zushi, Dr. Takumi Onchi

and fruitful discussions with Dr. Santanu Banerjee. Part of this research is with a collaboration with Prof. Shikama of Kyoto University, Kyoto.

**Publication and presentation**

H Idei, T Kariya, T Imai, K Mishra, T Onchi, O Watanabe, H Zushi, K Hanada, J Qian, A Ejiri, MM Alam, K Nakamura, A Fujisawa, Y Nagashima, M Hasegawa, K Matsuoka, A Fukuyama, S Kubo, T Shimozuma, M Yoshikawa, M Sakamoto, S Kawasaki, H Nakashima, A Higashijima, S Ide, T Maekawa, Y Takase, K Toi, "Fully non-inductive second harmonic electron cyclotron plasma ramp-up in the QUEST spherical tokamak", Nucl. Fusion 57, 126045

## 国際化推進共同研究概要

No.8

タイトル: Control of plasma generated by the new CHI system on QUEST

研究代表者: NELSON, Brian, A

所内世話人: 花田 和明

概要:

## Control of plasma generated by the new CHI system on QUEST \*

2 January 2018

R. Raman<sup>1</sup>, K. Kuroda<sup>2</sup>, K. Hanada<sup>2</sup>, T. Onchi<sup>2</sup>, H. Canbin<sup>2</sup>, M. Hasegawa<sup>2</sup>, M. Ono<sup>3</sup>, B.A. Nelson<sup>1</sup>, T.R. Jarboe<sup>1</sup>, M. Nagata<sup>4</sup>, O. Mitarai<sup>5</sup>

<sup>1</sup> University of Washington, Seattle, WA, USA

<sup>2</sup> Kyushu University, Kyushu, Japan

<sup>3</sup> Princeton Plasma Physics Laboratory, Princeton, NJ, USA

<sup>4</sup> University of Hyogo, Himeji, Japan

<sup>5</sup> Institute for Advanced Fusion and Plasma Education, Japan

### Introduction

Methods for starting a plasma discharge in a spherical tokamak (ST) without reliance of the center solenoid are essential for the validity of the ST concept. These methods could also simplify and reduce the cost of tokamak-based systems and make them more economical by eliminating components that are not needed during steady-state operation. Coaxial Helicity Injection (CHI) for an ST, first developed on HIT-II at the Univ. of Washington, is the leading method adopted by NSTX-U to generate the initial current during a planned full non-inductive current start-up and current ramp-up scenario. On QUEST, this method would be further developed using the unique all metal capability of QUEST, which is predicted to reduce low-z impurities. In addition, CHI on

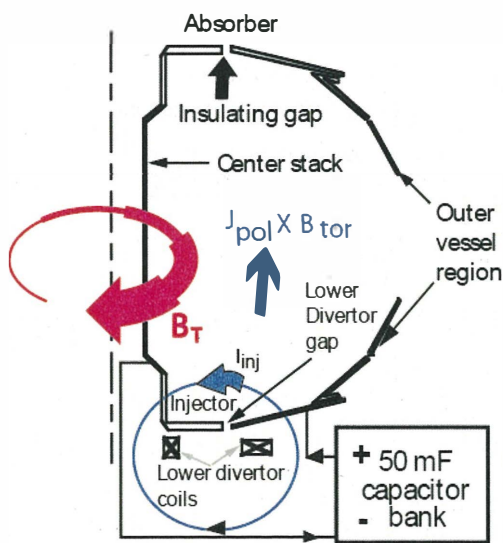


**Figure 1:** Layout of the transient CHI startup systems in NSTX. The blue circle is the poloidal injector flux produced by the lower divertor coils. This connects the two lower divertor plates, which are insulated. Gas is injected in the region below the divertor gap. On NSTX typically a 5 to 15mF capacitor bank charged up to 1.7kV is used to produce the injector current.

QUEST will develop a new configuration that is much more suited to ST-FNSF. CHI start-up on QUEST could be used to provide an alternate, and when combined with induction, higher current targets for RF current drive studies. There are a number of new and important studies that would be possible on QUEST. These are: (a) Benefits of high-power ECH for CHI discharge initiation and heating of CHI plasmas, (b) impact of an all metal wall configuration for reducing low-z impurities, and (c) development of a simpler electrode configuration that is much more suitable for a fusion reactor as described in the Reference [Raman, et al., *Fusion Science & Technol.*, **68** (2015) Pg. 674]. All these objectives are well aligned with the long-term mission of QUEST to develop steady-state fusion reactor technologies. This document discusses the near-term plans for CHI studies on QUEST.

\* We acknowledge helpful discussions with Prof. Zushi, Mr. Noda (V-Tech Limited) and Mr. Rogers (Univ. of Washington) and with other members of the QUEST Team.

## Basic concept for CHI operation on QUEST

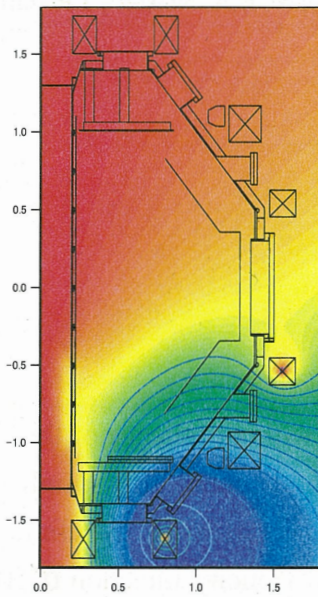


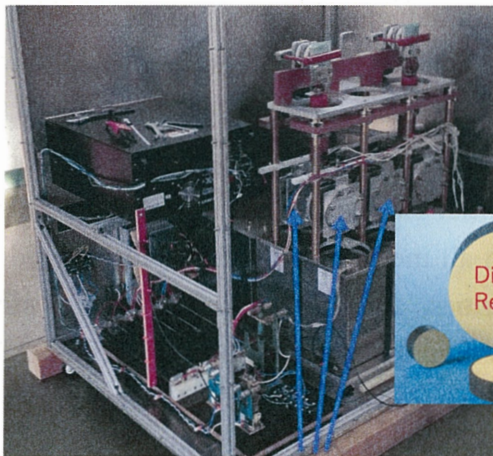
**Figure 2:** Typical magnetic surface at plasma production using CHI electrode. A continuous ring insulator electrically separates the cathode electrode from the lower divertor plate.

On QUEST, as briefly described in Fig. 2, a toroidal ring electrode is mounted on top of the existing lower divertor plate, and the electrode separated from the divertor plate using a toroidal alumina insulator. Magnetic flux generated by the lower divertor coils connect this electrode plate (the cathode) to the outer vessel (the anode). Gas is injected in the gap between these electrodes and a 20-30mF capacitor bank, charged up to 2kV is discharged across these electrodes to generate the CHI plasma.

## Progress with CHI on QUEST

During 2017, there were two CHI run campaign on QUEST, each two weeks long. During the first of these campaigns during May, the first week was spent improving the voltage monitoring system on the capacitor bank, re-testing the CHI capacitor bank and improving two fast CHI gas injection systems by using smaller gas injection plenums and increasing the operating pressure from 0.4 to 0.8 MPa. A new fast mid-plane camera system was also commissioned during CHI plasma discharges.

## CHI PS Resistor Change



12 - 150mOhm resistors will be replaced with 12 - 40mOhm resistors

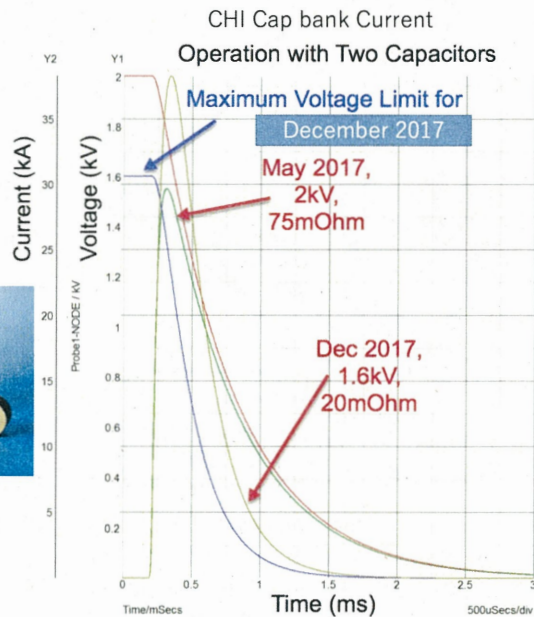


**Figure 3:** (Left) The high-power disk resistors were replaced in the CHI capacitor bank to permit faster ramp-down of the injector current. (Right) Calculations showing the changes to the capacitor bank current capability before and after the modifications.

This was followed by re-establishing discharges conducted during the December 2016 campaign. During the second week progress was made in four areas. First, the CHI produced toroidal current was increased from 29kA (in December 2016) to over 40kA. Second, the current multiplication

ratio (defined as the ratio of the CHI produced toroidal current divided by CHI power supply current) was increased from 0.75 to over 1.5. Third, during the design phase of the new biased electrode system for QUEST, it was believed that this configuration might be more prone to absorber arcs. During this run, improved camera measurements of the lower divertor region identified the occurrence of absorber arcs. Absorber arcs are undesirable discharges that should be minimized or avoided, as it provides another unbeneficial path for the current driven by the CHI power supply. However, through proper programming of the poloidal field coils, and gas injection conditions, these arcs were controlled. Fourth, absorber arc control allowed us to initiate discharges in a near-narrow injector flux footprint configuration, with the use of strong vertical fields, to conduct useful scans of the effect of the vertical field, the effect of increases to voltage application, and the impact of operating with a single gas valve.

A primary objective for the second campaign in December was to observe toroidal current persistence after the CHI injector current was reduced to zero. Based on results from the May run campaign, it was determined that to achieve this goal it was necessary to more rapidly reduce the injector current after the CHI plasma was initiated. To enable this capability in the CHI power

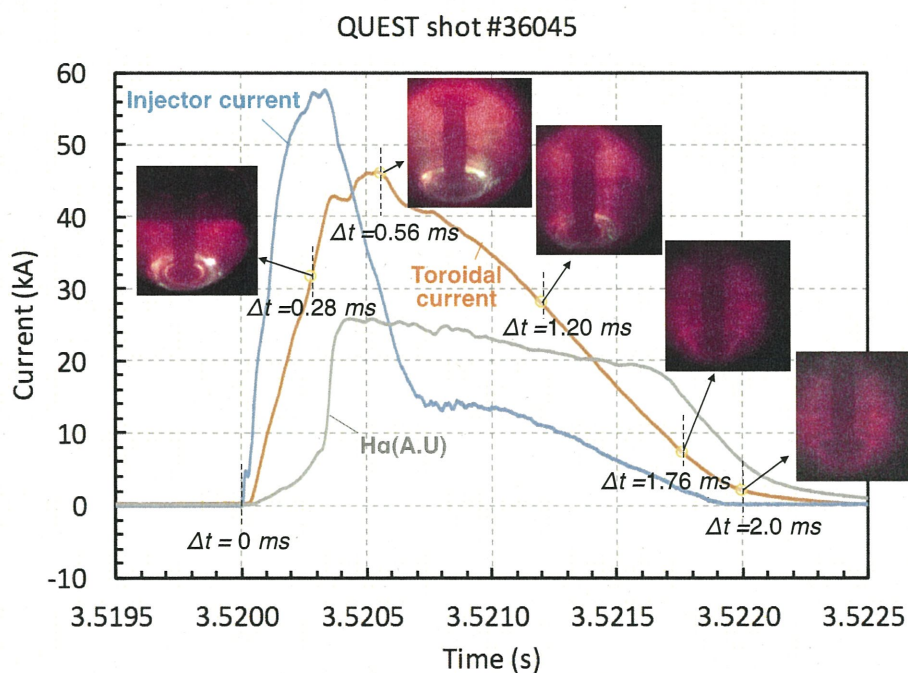


**Figure 4:** CHI produced toroidal current, CHI injector current, Halpha signal, and fish eye fast camera images at different times during the discharge.

supply, the Univ. of Washington team spent the first four days partially disassembling the CHI capacitor bank and replacing twelve current limiting power resistors from 150 mOhms to 40 mOhms (Figure 3). With this modification, additional software and hardware based protection measures were implemented to limit the maximum operating voltage to 1.6kV (from 2kV).

Then, during the course of the next few days, based on the observed experimental results, additional hardware changes were made to the CHI and QUEST systems. The volumes of the CHI gas plenums were systematically reduced so that much less gas was injected per pulse. The power supply configurations for the QUEST PF coils were also changed to provide better control of the CHI plasma discharges. A fast color camera from PPPL (on loan to QUEST) was used to obtain full coverage of the CHI plasma growth into the vessel. With these numerous changes, two important improvements were made to the transient CHI discharge. First, the total amount of

injected gas was reduced by a factor two compared to the gas injection amounts used during the May campaign and to 16% of the gas injection amounts used during the very first CHI discharges on QUEST. Initiation of CHI discharges at sufficiently low levels of injected gas is quite important, and necessary, as described in a recent NSTX CHI paper (K.C. Hammond, et al., 2018 Nuclear Fusion **58** 016013). With these hardware improvements above, improved toroidal currents up to 50kA were generated that showed toroidal current persistence after the injector current was reduced to zero (Figure 4). The reliability of absorber arc-free CHI discharges also considerably improved, even though much less fuel gas was injected during this run. The run campaigns during May and December have allowed us to make good steady progress towards developing the new CHI electrode configuration for future application to a ST based reactor.

## 国際化推進共同研究概要

No.9

タイトル: Towards high mode purity in ECRH transmission lines for ITER

研究代表者: KASPAREK, Walter, Hermann

所内世話人: 出射 浩

概要: トカマクにおける不安定性抑制には、揺動の回転に同期した電子サイクロトロン電流駆動が有効であることが示されている。回転周波数が 10kHz 程度であることから、これまでの同期手法は入射電力のオン・オフであった。近年、入射位置のスイッチングにより同期手法が検討されている。2 周波数の電子サイクロトロン電流駆動の入射位置のスイッチングにつき、これまでの検討の検証と、さらにその評価法の再検討を進めた。

# Towards high mode purity in ECRH transmission lines for ITER

Applicant: Walter Kasperek

Institute of Interfacial Process Engineering and Plasma Technology (IGVP)

Electron Cyclotron Heating (ECH) using high power millimetre waves is an attractive method for plasma production, auxiliary heating, and current drive in a nuclear fusion research. Accordingly, the ECH system at the International Thermonuclear Experimental Reactor (ITER) will have a total injected power of 20 MW at an operating frequency of 170 GHz. For 20 MW injections to the plasma, 24 high-power gyrotron oscillators of 14 MW each will be used. The output beam from each gyrotron oscillator is led to a Circular Corrugated (CC) waveguide line, and transmitted as an  $HE_{11}$  mode of a main eigen-mode in the waveguide. 24 CC waveguide lines will be prepared to transmit the total 20 MW power. Excitation of unwanted higher-order modes in the oversized waveguide causes many problems such as excessive transmission loss, arcing, thermal overload of components due to stray radiation, and finally deviations of the launched beams from the nominal direction. In earlier works, transmission losses in the ITER ECH system due to higher-order mode excitation in misaligned components have been estimated, and the impact on the launched beams was studied.

This collaboration has been established to excite and transmit the high-purity main  $HE_{11}$  mode under monitoring and controlling of the transmitted wrong modes for the CW high power application.

The International Joint Research team consisted (besides the applicant) of Hiroshi Idei (RIAM, Kyushu), Keishi Sakamoto (JAEA Naka), Takashi Shimosuma (NIFS, Toki), Richard Temkin (MIT PSFC Cambridge), Michael Shapiro (MIT PSFC Cambridge), Alexander Zach (IGVP Stuttgart), Carsten Lechte (IGVP Stuttgart), and Burkhard Plaum (IGVP Stuttgart).

## Investigations of the beam splitting performance of a square corrugated waveguide

Burkhard Plaum, Hiroshi Idei

For JT-60 a high power capable resonant diplexer for the frequency bands around 110 GHz and 137.55 GHz is designed. It is based on square corrugated waveguides (SCWs), which act as beam splitters. These splitters can be combined with phase reversing mirrors and arranged in a sequence to form ring resonators [1].

In the traditional approach, an SCW, which is fed by a Gaussian beam under a small angle  $\theta_{in}$ , acts as a beam splitter if the length  $L$  is chosen as

$$L = \frac{2a^2}{\lambda}$$

with the waveguide width  $a$  and the free space wavelength  $\lambda$ . If one investigates, however, a larger range of lengths and angles, additional branches can be found, where a beam splitting behavior is observed. These higher branches are necessary to realize a beam splitter, which works in two frequency bands.

In order to search for good operating parameters, we need to define a figure of merit which indicates the quality of a beam splitter. For this, we calculate the field distribution at the end of the waveguide and calculate the power contents  $p_1$  and  $p_2$ , which correspond to the beams radiated under  $\theta_{in}$  and  $-\theta_{in}$  respectively. The beam parameters (e.g. the Gaussian waist radius  $w_0$ ) at the

output are assumed to be identical to the input beam. Note that in reality the beam parameters change slightly and side lobes are radiated. This means that typically  $p_1 + p_2 < 1$ . Also,  $p_1$  and  $p_2$  are real numbers because the relative phase between the two beams is not relevant. Once  $p_1$  and  $p_2$  are calculated, the figure of merit (FOM) is derived as:

$$FOM = p_1 + p_2 - |p_1 - p_2|$$

The first term requests the total power in the beams to be as high as possible. This automatically prefers solutions, which have low side lobes and beam parameters similar as the input beam. The second term demands a symmetric power splitting ratio. Figs 1 and 2 show the FOM calculated from 110 GHz and 138 GHz respectively with the parameters suggested in [1].

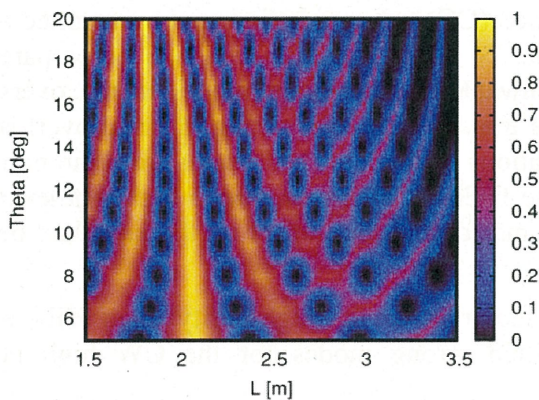


Fig 1: FOM calculated for 110 GHz

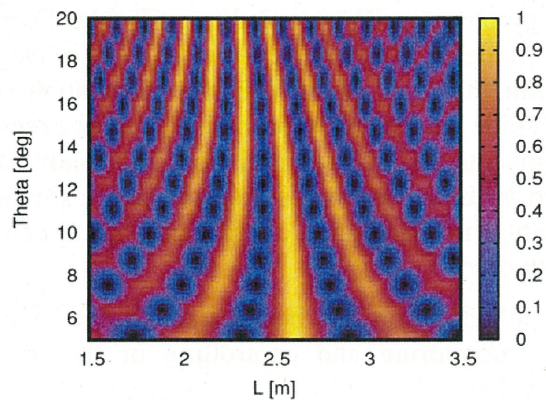


Fig 2: FOM calculated for 138 GHz

For the suggested parameters ( $L = 2.0$  m and  $\theta_{in} = 17.5^\circ$ ) the radiated fields at a distance of 0.2 m were calculated with PROFUSION and compared with the results from [1]. Figures 3-5 show the results. One can see, that between both codes there is a perfect agreement even though different methods were used for calculating the propagation.

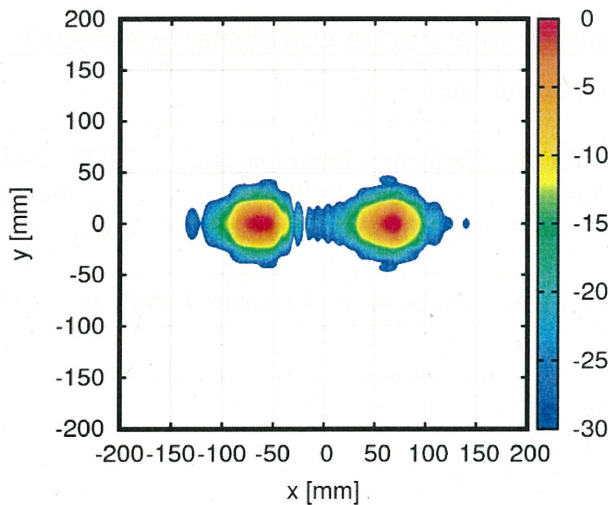


Fig 3: Radiation pattern calculated with the FFT algorithm from PROFUSION at 110 GHz

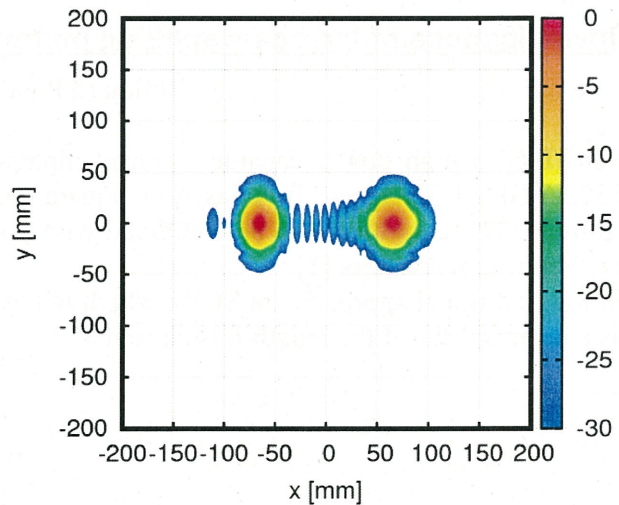


Fig 4: Radiation pattern calculated with the FFT algorithm from PROFUSION at 138 GHz

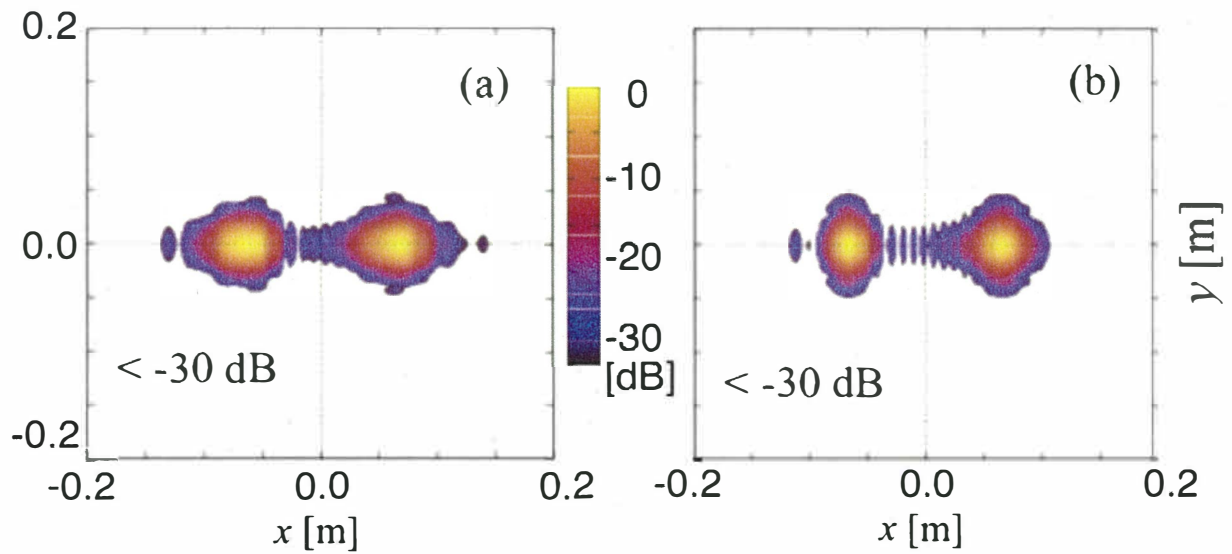


Fig 5: Radiation pattern calculated with the Kirchhoff Integral method for 110 GHz (left) and 138 GHz (right) [1]

The horizontal intensity and phase profiles of the field patterns are shown in Figs 6-8. The agreement is, again, perfect.

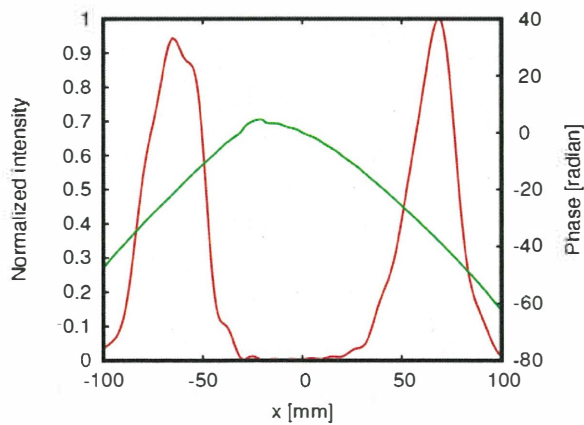


Fig 6: Horizontal intensity- and phase profile calculated with the FFT algorithm from PROFUSION at 110 GHz

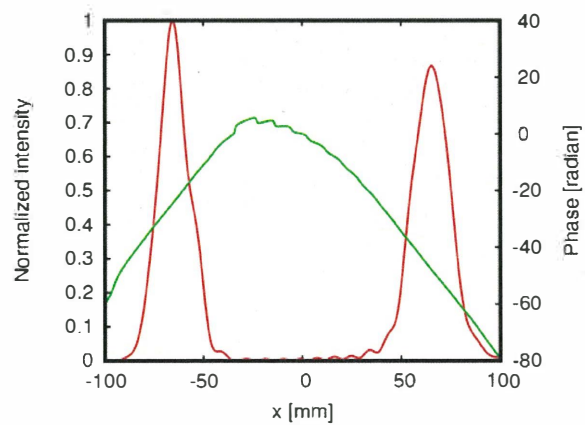


Fig 7: Horizontal intensity- and phase profile calculated with the FFT algorithm from PROFUSION at 138 GHz

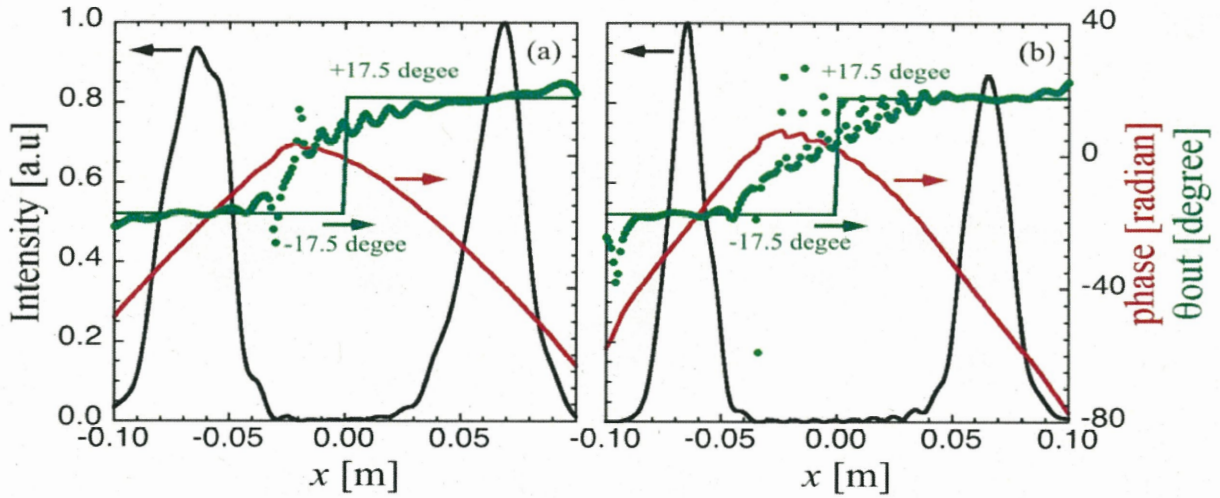


Fig 8: Horizontal intensity- and phase profile calculated with the Kirchhoff Integral method for 110 GHz (left) and 138 GHz (right) [1]

After verifying the codes, we look for final design parameters. First, the exact value for the second frequency changed to 137.55 GHz. The criterion for the waveguide width is, that the beam sizes should be comparable in the cylindrical  $HE_{11}$  transmission line and in the SCW. This simplifies the design of the coupling mirrors later on. By varying the width of the SCW and calculating the overlap integral of the  $HE_{11}$  modes in both waveguides, we find a maximum at 55.3 mm. The waist radius of a corresponding Gaussian beam is 19.4 mm.

With these parameters we calculate the FOMs for both frequencies the same way as in Figs 1 and 2. Since the beam splitter should work equally well in both frequency bands, we can define a total figure of merit  $FOM_{total}$  the following way:

$$FOM_{total} = FOM_{110} + FOM_{137.55} - |FOM_{110} - FOM_{137.55}|$$

Fig. 9 shows the calculated  $FOM_{total}$ . We identify a parameter range around  $L = 2.14$  m and  $\Theta_{in} = 16.6^\circ$  as best operating area. To further refine the values we do a second parameter scan with finer resolution in the rectangular area in Fig. 9. The result is shown in Fig. 10. The new optimum is now located at  $L = 2.146$  m and  $\Theta_{in} = 17.85^\circ$ .

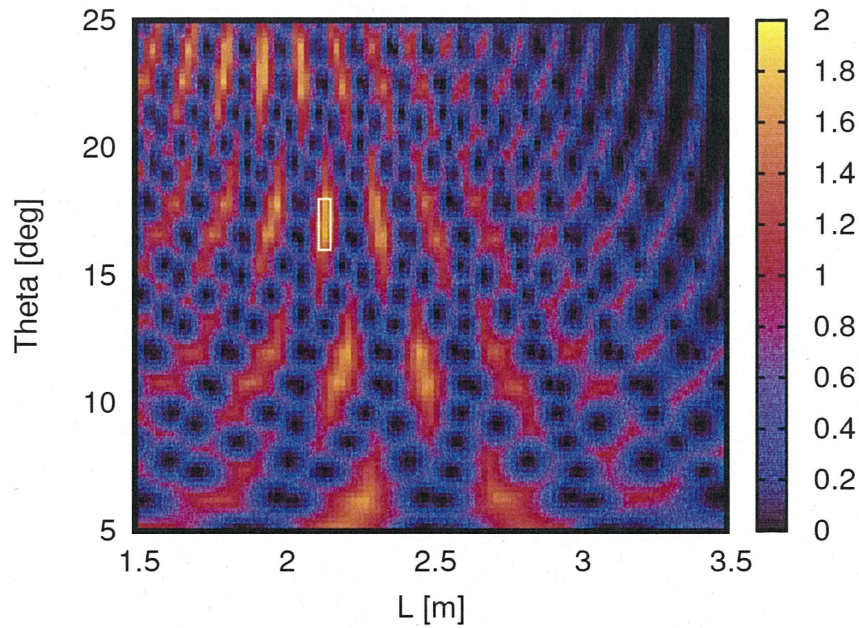


Fig 9: Total FOM with the window, where a finer scan will be performed

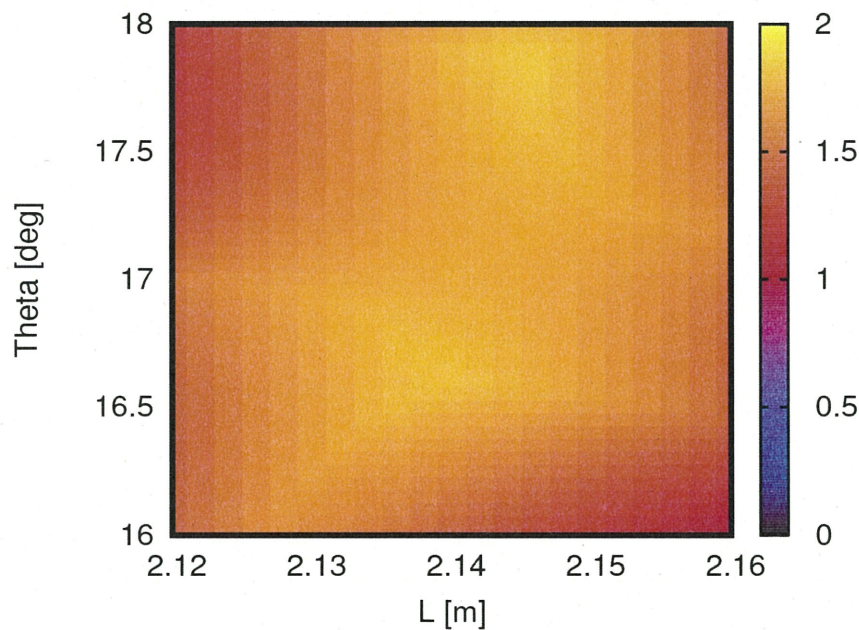


Fig 10: Total FOM calculated with finer resolution

Further work will be the fine tuning Gaussian waist radius and the analysis of the radiated beams.

[1] H. Idei, T. Kobayashi, S. Moriyama, A. Isayama, M. Sakaguchi, W. Kasparek, *Conceptual Design of Dual Baseline-Frequency Fast Directional Switch using Square Corrugated Waveguide Splitter/Combiner*, J Infrared Milli Terahz Waves (2015) 36:662–674

## 国際化推進共同研究概要

No.10

タイトル: Plasma start-up and sustainment in spherical tokamak configuration by RF

研究代表者: SHEVCHENKO, Vladimir

所内世話人: 出射 浩

概要: 英国の研究者が座長するワークショップにて、球状トカマクで重要となる非誘導電流駆動につき、英国の ST40、米国の NSTX 装置、日本の LATE 装置、TST 装置、QUEST 装置における非誘導電流駆動の研究成果を議論し、今後の QUEST 装置実験計画について意見交換した。QUEST 装置からは、最近の 28GHz システムを用いた非誘導電流駆動の研究成果が示された。参加者は英国から 1 名、米国から 3 名、日本からは数名であった。

RF-only ST plasma confinement, sustainment,  
and interactions with wall materials

**Hiroshi Idei**

**Vladimir Shevchenko**

A program of the Workshop which was held on 1-2 February 2018 and was as following:

**6<sup>th</sup> Workshop Agenda, RIAM 2018**

*1 February AM*

9:30 -9:40

Vladimir Shevchenko / Kazuaki Hanada

**WS purpose and agenda**

9:40 - 10:30

Vladimir Shevchenko

**ECRH and ECCD Potential on ST40**

10:30 - 11:10

Hiroshi Idei

**Progress and Plans on Non-Inductive Plasma Current Ramp-up Experiment in QUEST**

Additional

Hatem Elserafy

**HFS injection for EBW excitation in QUEST**

11:10 - 11:20

**Coffee Break**

11:10 - 11:50

Satoru Yajima

**Comparison of Ip Start-up by Outboard-Launch and Top-Launch LHW on TST-2**

11:50 - 12:20

Yuichi Takase

**LH Ip Start-up Experiments on TST-2: Past and Future**

12:20 - 13:00

Masayuki Uchida

**Progress and Plans of LATE Experiments (Tentative)**

*1 February PM*

14:30 - 15:20

Masayuki Ono

**Status of NSTX-U recovery and solenoid-free start-up / current ramp-up program**

15:20 - 16:00

Nicola Bertelli

**Initial & preliminary Fokker-Planck simulations by using the CQL3D code for QUEST plasmas**

16:00 - 16:40

Luis F. Delgado-Aparicio

**Multi-energy SXR imaging and its applications to QUEST plasmas**

**16:40 - Group Photo & QUEST Machine Tour**

*2 February AM*

9:30 - 10:10

Kengoh Kuroda

**CHI Experiments in QUEST**

10:10 - 10:50

Taiichi Shikama

**Spectroscopic measurements of intrinsic toroidal rotation in QUEST**

10:50 - 11:30

Sadayoshi Murakami

**Simulation study of toroidal flow generation by ECH in non-axisymmetric toroidal plasmas**

11:30 - 12:10

Shin Kubo

**Plan for a direct detection of EBW by sub-THz gyrotron scattering in QUEST**

*2 February PM* (Drafting of proposals for experiments, diagnosis, and analysis)

14:00 - **All Suggested focus and output for this joint drafting session**

16:30 - Vladimir Shevchenko

**Summary**

---

## The presentation summaries are as following:

### Vladimir Shevchenko, ECRH and ECCD Potential on ST40

Overview of present status of the ST40 project was presented. Main objectives of the project, parameters of the tokamak, physics program issues are described, and physics and engineering challenges of this device are discussed. A set of ST40 diagnostics were discussed briefly. Fast cameras, visible and UV spectroscopy, magnetics and dual color interferometry were installed on the machine for the first plasma operation.

ST40 power supplies for toroidal field, merging compression coils, vertical field and divertor coils are currently under commissioning. However, first plasma has been achieved in ST40 using merging compression technique in a relatively low toroidal field of 0.3T. Plasma currents up to 30kA have been measured transiently even in the absence of vertical field. Merging compression plasma formation with vertical field will be attempted this week during commissioning of the vertical field power supply.

ECRH and ECCD have a great potential in ST40. During full scale operation the magnetic field should reach 3T at the magnetic axis. This corresponds to the frequency of 170GHz for the second EC harmonic at the plasma centre. Gyrotrons with output power up to 1MW are widely available for this frequency (developed for ITER). Detailed ray-tracing and Fokker-Planck modelling has been conducted for ST40 around fundamental EC resonance and second harmonic EC resonance. It was found that heating and current drive can be achieved at both harmonics. For the fundamental EC resonance RF power around 84GHz must be launched from the high field side (HFS), which possible in ST40 but technically challenging. Second EC harmonic allows more convenient low field side (LFS) launch at the frequency around 170GHz. In both configurations the current drive efficiency around  $\eta_{20} = 40 \text{ kA} \cdot 10^{20} \text{ m}^{-3} \cdot \text{keV}^{-1}$  is expected. However, the HFS launch can also provide very efficient non-inductive plasma start-up and current ramp-up while LFS launch requires presence of the optically thick plasma in the vessel. Both options are considered for potential use on ST40 in addition to NBI heating.

### Hiroshi Idei, Progress and Plans on Non-Inductive Plasma Current Ramp-up Experiment in QUEST

The EC heating and current drive (ECHCD) system with a 28 GHz gyrotron has been prepared for non-inductive EC plasma ramp-up in the QUEST. Non-inductive plasma start-up using the EC waves is a key issue for advanced tokamak reactor concepts as well as for the ST concept. There are two important aspects of conducting the present ECHCD current ramp-up experiments. One is a beam focusing, and the other is incident polarization control. A new transmission line (TL) and an antenna system composed of polarizers and a large focusing mirror has developed for the local ECHCD. The waist-size of the launched beam was about 0.05 m at the ECR layer. The incident beam can be steered from perpendicular to tangential injection. The steering capability with focusing property was confirmed at the low power test facilities. The local ECHCD effect was observed with the focusing beam in the incident polarization scan. The 86 kA plasma current was achieved using the new TL and launcher. The right-hand cut-off density  $n_{\text{cut}}$  of the 2nd harmonic 28 GHz-wave is  $\sim 3 \times 10^{18} \text{ m}^{-3}$  for the oblique injection with  $N_{\parallel} = 0.78$  at the ECR layer. The temperature  $T_e$  decreased with the increasing  $n_e$

beyond the cutoff density, then the HX count started to increase. The HXs with 60 keV energy range were measured at the forward tangential viewing radius of 0.32 m for current-carrying electrons. Electron density was one order of magnitude higher compared to the previous experiments with no beam focusing. The current might be generated by energetic electrons, accelerated at the relativistic Doppler-shifted resonance, due to the local ECHCD effect with the incident focused beam, as well as the multiple reflection effect after the cut-off.

#### **Hatem Elserafy, HFS injection for EBW excitation in QUEST**

This presentation contains the High Field Side (HFS) injection scenario for QUEST spherical tokamak. There are several methods for Electron Bernstein Wave (EBW) excitation including O-X-B (Ordinary-eXtranordinary-Bernstein) mode conversion injected from the Low Field Side (LFS), and X-B (eXtraordinary-Bernstein) mode conversion injected from the HFS. O-X-B mode conversion from LFS was attempted in QUEST without any successful EBW conversion. The primary issue was aligning the injection antenna with the polarizing mirror at the HFS that is responsible of the conversion from O-mode to X-mode. X-B mode conversion takes it one step closer, which guarantees not to suffer from the alignment problem. X-B mode was proposed in previous literature mentioning conversion efficiency from X-mode to EBW of 100% at the upper hybrid resonance (UHR) layer. However, those systems used mirrors to transmit the wave to the HFS causing undesired power loss. Our proposed system is to extend the waveguide all the way from the LFS to the HFS to maximize power transmission. One drawback is that the waveguide has to pass through the ECR layer and will induce breakdown inside of the waveguide. To avoid that problem, the waveguide will be filled with SF<sub>6</sub> gas to suppress breakdown, while using a sapphire safety window to prevent SF<sub>6</sub> leakage inside the vessel. This scenario was externally tested using an electromagnet to emulate the ECR layer and 12 kW were successfully transmitted without arcing. Another problem that might arise is the wave absorption at ECR layer, decreasing the amount of power reaching UHR, and thereby decreasing the efficiency. To tackle this problem, optical absorption coefficient was calculated in order to design the horn antenna parameters. The optical absorption dictates that the antenna should be highly directive in order to maximize conversion efficiency at the UHR. However, due to physical space limitation, the antenna has to be as compact as possible. Antenna size was optimized trading off size and directivity, and the experiment is yet to be conducted. Future plans include integrating 2 other klystrons, and reverting plasma current based on antenna location.

#### **Satoru Yajima, Comparison of Ip Start-up by Outboard-Launch and Top-Launch LHW on TST-2**

Significant increase of the plasma current and the soft X-ray intensity is obtained by top injection. So far, achievable current is 21.5 kA by outboard launch and 26.7 kA by top launch with top limiter position of  $z=350$  mm and bottom limiter position of  $z=-390$  mm.

GENRAY/CQL3D calculation showed the different characteristics among top, outboard, and simulated bottom injection (TF CCW with top launch). Top launch can extend the tail of velocity distribution by the absorption in wide parallel wavenumber range. Simulated bottom launch can further extend the tail due to initial downshift in wavenumber.

Achievable plasma current is mainly proportional to  $B_t$ , but top & bottom limiter can reduce the plasma current and induce fast electron loss.

From full wave calculation

Top launch: Optimum distance between antenna and plasma is 17-27 mm

Outboard launch: Reflection is suppressed when the limiter is displaced 70 mm

### Yuichi Takase, LH $I_p$ Start-up Experiments on TST-2: Past and Future

ST plasma initiation and  $I_p$  ramp-up by the lower hybrid wave (LHW) were demonstrated on the TST-2 spherical tokamak. Progressive improvements in the achieved  $I_p$  were accomplished using different methods of wave excitation. High wave directivity of the newly-developed capacitively-coupled combline (CCC) antenna was confirmed by the co/counter asymmetry of hard X-ray emission. Since numerical modeling indicates  $n_{||}$  upshift and strong single-pass absorption for top-launched LHW, the top-launch CCC antenna was installed in addition to the outboard-launch CCC antenna. In LHW-driven plasmas, both  $p_e$  and  $j$  are dominated by energetic electrons,  $n_e$  profile is peaked whereas the  $T_e$  and  $j$  profiles are hollow, and the driven  $I_p$  increases with  $n_e$ , and higher  $n_e$  requires higher  $B_t$ . The top-launch LHW is found to be more effective than the outboard-launch LHW for both directions of  $B_t$ , and  $I_p$  ramp-up to  $> 25$  kA has been achieved with less than 100 kW of RF power. The improvements being considered based on numerical modeling include: TF power supply upgrade to enable higher  $B_t$  for longer pulse, optimization of launcher positions and  $n_{||}$  spectra, 3-D control of wavevector (toroidal and poloidal wavenumbers), combination of 450 MHz (for core heating) and 200 MHz (for current drive), and reduction of SOL losses by improved single-pass damping. Since orbit losses of high energy electrons should decrease at higher  $I_p$  and  $n_e$ , a substantial improvement in the  $I_p$  ramp-up efficiency may be possible

### Masayuki Uchida, Progress and Plans of LATE Experiments

Highly overdense plasma is non-inductively started up and sustained by ECH/ECCD by EB waves mode-converted in their first propagation band. The electron density reaches  $6 \times 10^{17} \text{ m}^{-3}$  which is  $\sim 8$  times the plasma cutoff density, where  $I_p$  reaches 12 kA by injecting 2.45GHz power of 65kW. In the 5GHz 70kW experiment, the electron density reaches  $1.5 \times 10^{18} \text{ m}^{-3}$  which is  $\sim 5$  times the plasma cutoff density, where  $I_p$  is ramped-up to  $\sim 9$  kA. EBW heating with multi-EC resonances using both the 2.45GHz and 5GHz microwaves is demonstrated during the non-inductive start-up. A 5GHz power of 70 kW is injected into a plasma of  $n_e \sim 5 \times 10^{17} \text{ m}^{-3}$  and  $I_p = 8.5$  kA which is generated by the fundamental EBW heating with a 2.45GHz power of 35kW. The plasma current increases up to 14kA with a significant increase of HX emission intensity, suggesting a current carrying fast electron tail is strongly developed by the 2nd harmonic EBW heating of the 5GHz power.

## Masayuki Ono, NSTX-U Plasma Start-up Research Program and Collaboration Strategy

National Spherical Torus Experiment Upgrade is a low-aspect-ratio ( $A \sim 1.6 - 1.8$ ) spherical tokamak facility at PPPL with  $B_T \sim 1$  T,  $I_p \sim 2$  MA,  $P_{NBI} \sim 14$  MW, and  $P_{RF} \sim 4$  MW. The unique operating regimes of NSTX-U can contribute to important physics issues for the ST development path. After the PF-1A (a divertor control coil) failure, a recovery project was formed. A number of internal and external reviews were conducted, and it was concluded that the NSTX-U lower ceramic insulation will be removed which preclude the conventional coaxial helicity injection (CHI) capability. This resulted in a reexamination of our plasma start-up program. The NSTX-U Ramp-Up studies will continue using inductively generated targets with HHFW & NBI, as in original plan. NSTX-U solenoid-free start-up activities will be conducted in other ST facilities in the near term: The NSTX-U team will support the more reactor relevant CHI research being conducted on QUEST. If successful, it would be possible to implement an CHI system on NSTX-U without toroidally continuous ceramic insulator. It should be also noted that the PEGASUS group is developing the localized helicity injection (LHI) system. The NSTX-U team would like to enhance collaboration on ECH / EBW start-up studies being conducted on QUEST through theory/modeling and multi-energy soft x-ray camera collaborations. The ultimate goal of NSTX-U is to start-up and sustain high  $\beta$  plasma fully non-inductively without use of central solenoid.

## Nicola Bertelli, Initial & preliminary Fokker-Planck simulations by using the CQL3D code for QUEST plasmas

1. Performed initial Fokker-Planck CQL3D simulations for QUEST plasma
  - a. Parabolic profiles
  - b. Work still in progress
2. Found very strong tail representing high energetic electrons on the location of 2<sup>nd</sup> harmonic resonance
3. Total current driven by high energy electrons lower than experiment
  - a. Probably need to improve some parameters for the simulations

### COLLABORATION with QUEST

#### Tasks:

- 1) Continue work on CQL3D simulations in collaboration with Idei-sensei
  - a. More realistic data (?)
  - b. Different dispersion relations
- 2) Comparison of SXR data with CQL3D synthetic diagnostic
  - a. Including future data from Luis F. Delgado-Aparicio's camera

- 3) Collaboration also with R. Harvey (waiting answer from a proposal to work on QUEST submitted in 2017)

Luis F. Delgado-Aparicio, Multi-energy SXR imaging and its applications to QUEST plasmas

Summary points for QUEST talk:

- Measurement of power losses in the x-ray range enables the characterization of local plasma parameters to study MHD, transport and confinement.
- Multi-energy SXR/HXR diagnostic probes mainly the electron channel (e.g.  $T_e$  and  $n_{e,fast}$ ) but also  $n_z$ ,  $\bar{Z}_{eff}$  and  $Z_{eff}$  from the continuum & line-emission.
- Pilatus3 technology allows for individually selecting (64) energy ranges from 1.6 keV and above for all its 100k pixels (minimum).
- New imaging concept based on PILATUS3 detectors combines best features from PHA & multi-foil methods
- ME-SXR systems can also be used at QUEST for studying the fast-electron emission between 2 and 30-40 keV.
- Limitation of Si above 20-30 keV. Use CdTe up to  $\sim 100$ -200 keV.

Kengoh Kuroda, CHI Experiments in QUEST.

Quest is developing a new design CHI electrode configuration that is more suitable for a fusion reactor.

- Reliable discharge initiation successfully obtained with the new design electrodes on QUEST.

However, some improvements were needed to achieve appropriate evolution for forming a closed flux surface.

- By improving capacitor bank power supply and PF coil programming, the plasma evolved closer to the appropriate shape, in which toroidal current increased up to 46kA and a large plasma persisted for a short time after the injector current decreased to zero.

Taiichi Shikama, Spectroscopic measurements of intrinsic toroidal rotation in QUEST

We measured toroidal and poloidal flow velocities of  $C^{2+}$  and  $O^+$  ions in QUEST using an optical emission spectroscopy system equipped with multiple viewing chords. In 8.2 GHz (IL) and 28 GHz discharges, the toroidal and poloidal velocities of these ions were less than 10 and 1 km/s, respectively. Among the possible driving and damping mechanisms, we investigated the effects of charge-exchange momentum loss by atoms and thermal ion loss-cone. As for the former, we found that the friction force by charge exchange increases at the outboard side, so that small velocity there could be a

consequence of atom penetration. The latter effect was checked by calculating the ion loss-cones using ion orbit calculation. The ensemble averaged toroidal velocity became larger for  $O^+$  than  $C^{2+}$  by a few km/s in the edge region, and this may explain observed velocity difference between  $C^{2+}$  and  $O^+$  ions.

#### **Sadayoshi Murakami, Simulation study of toroidal flow generation by ECH in non-axisymmetric toroidal plasmas**

The important role of the plasma flow and its shear in the transport improvement is suggested by many experimental observations. The spontaneous toroidal flow driven by ECH was observed in many tokamak and helical devices. In LHD, when ECH was applied to the NBI heated plasma, the toroidal velocity profile changed drastically and turned over in the core region. ECH generates a radial flux of suprathreshold electrons in non-axisymmetric plasmas. We assume that the energetic electron current enhances the bulk ion current to cancel the electron current, and the  $j \times B$  torque has a significant role in generating a toroidal flow. In this study, we investigate the roles of the  $J \times B$  torque due to the radial current of energetic electrons and the collisional torque by the energetic electrons, and compare with the LHD experiment results. As a result, the  $J \times B$  torque generated by ECH has the same order as the NBI torque, and its direction is opposite to NBI torque in the inner region. Also, we evaluate the torque by ECH in the tokamak with finite toroidal field ripple. We find that the significant torque by ECH is obtained in the case the toroidal field ripple  $> 0.1\%$ .

#### **Shin Kubo, Plan for a direct detection of EBW by sub-THz gyrotron scattering in QUEST**

The electron Bernstein wave (EBW) heating/current drive is the most attractive method in QUEST, because EBW can propagate over the cut-off density and give a chance to drive current steadily at over the cut-off density. Since the EBW can be excited through mode conversion process, it is important to clarify and optimize the injection condition by checking the excited EBW near the core region.

Direct detection of the density fluctuations associated with the EBW is planned. Expected wavenumber in the perpendicular to the magnetic field ranges  $10^4$ - $10^5$   $m^{-1}$ . The direct and detailed measurement of the density fluctuation associated with the EBW gives clear evidence of the excited EBW inside the core, since it is an electro-static wave. Such measurement can be performed by measuring the sub-Tera-Hz wave scattering. The adoption of Littrow mount grating enables flexible scattering configuration under limited port access.

Sub-THz gyrotron at 300-400 GHz gyrotrons at the power level of more than 50 kW have been developed in the Univ. of Fukui. One of such gyrotrons is planned to be introduced in the the QUEST as well as highly sensitive detectors developed for CTS in LHD.

#### **Several Proposals were submitted:**

**Luis F. Delgado-Aparicio:**

PPPL scientists (Luis F. Delgado-Aparicio with Nicola Bertelli and Masayuki Ono) are establishing collaboration with scientists at Kyushu University to discuss the possibility of installing a Multi-Energy Soft X-ray (ME-SXR) system at QUEST. A silicon PILATUS3 detector can be used to resolve details of SXR emission between 2 and 30 keV with adequate time-resolution (~1 ms), excellent spatial resolution (~1-2 mm) and coarse photon energy (~500 eV) resolution. This new imaging capability can support experiments aiming at studying start-up and sustainment of non-inductive plasma current in spherical tokamaks. Delgado-Aparicio has requested a tangential view aligned with the equatorial midplane at QUEST in order to circumvent the complications from performing a conventional (radial) poloidal tomography. A parallel activity will take place to obtain a synthetic non-Maxwellian x-ray spectra using CQL3D.

**Nicola Bertelli:**

All the codes above can be used for EC/EBW studies on QUEST plasmas under the collaboration between NSTX-U and QUEST teams.

**Tasks:**

- 1) Continue work on CQL3D simulations in collaboration with Idei-sensei
  - a. More realistic data (?)
  - b. Different dispersion relations
- 2) Comparison of SXR data with CQL3D synthetic diagnostic
  - a. Including future data from Luis F. Delgado-Aparicio's camera
- 3) Collaboration also with R. Harvey (waiting answer from a proposal to work on QUEST submitted in 2017)

## 国際化推進共同研究概要

No.11

タイトル: Electron Bernstein wave heating with XB mode conversion from low field side launch.

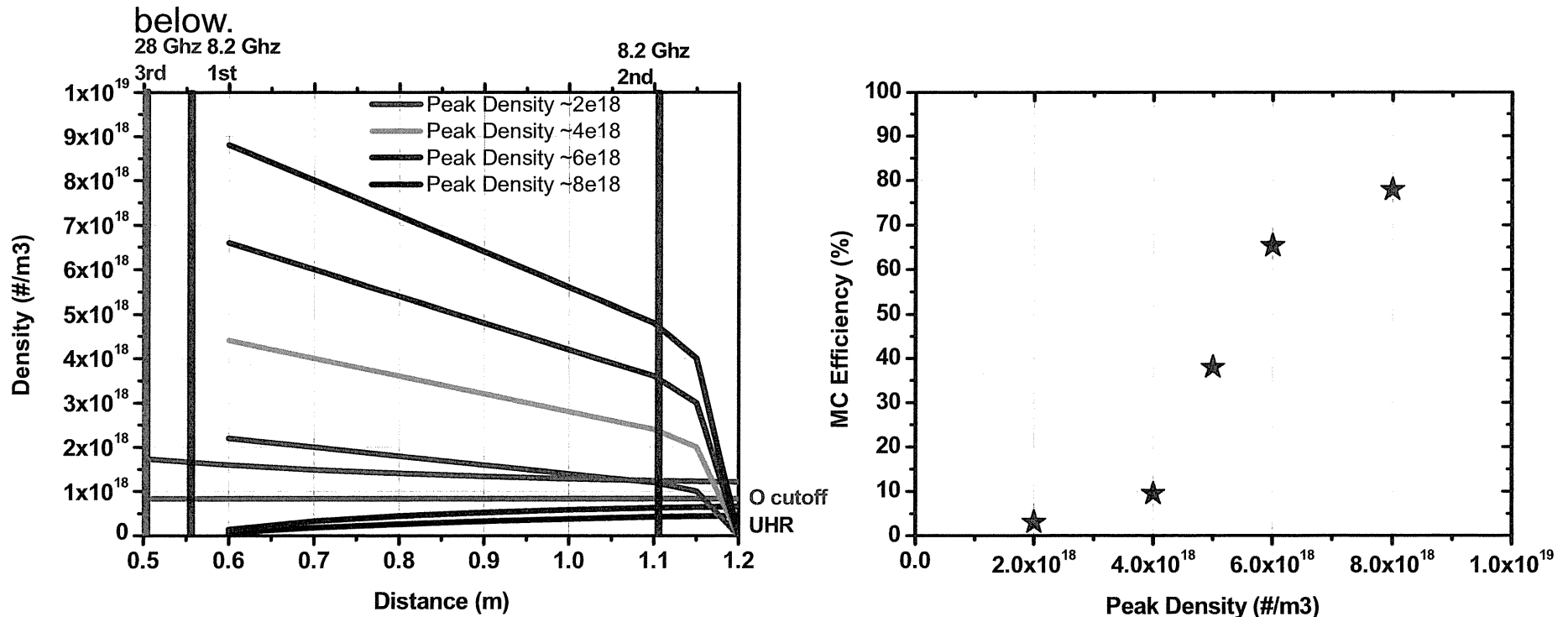
研究代表者: Hwang, Yong-Seok

所内世話人: 花田 和明

概要:

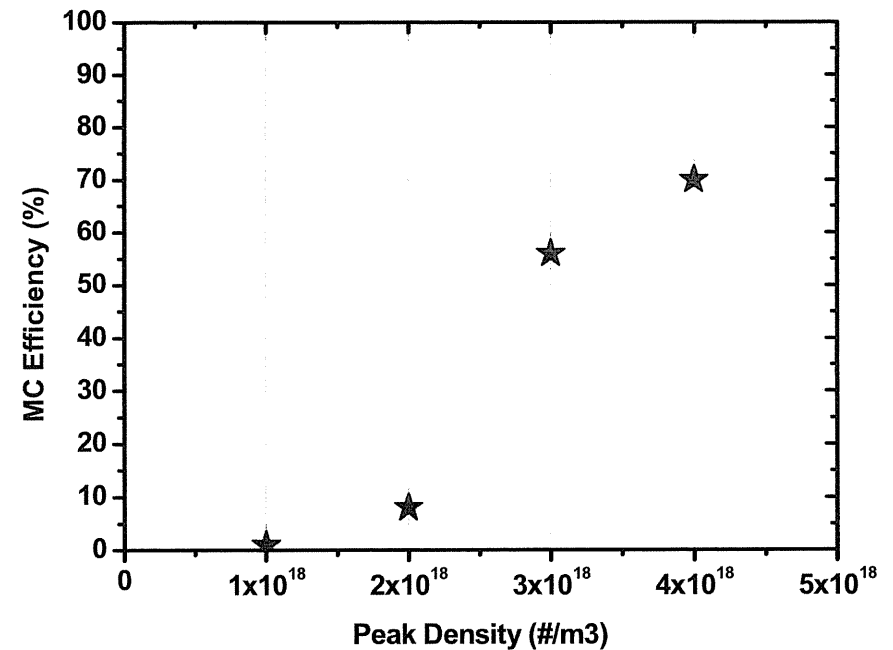
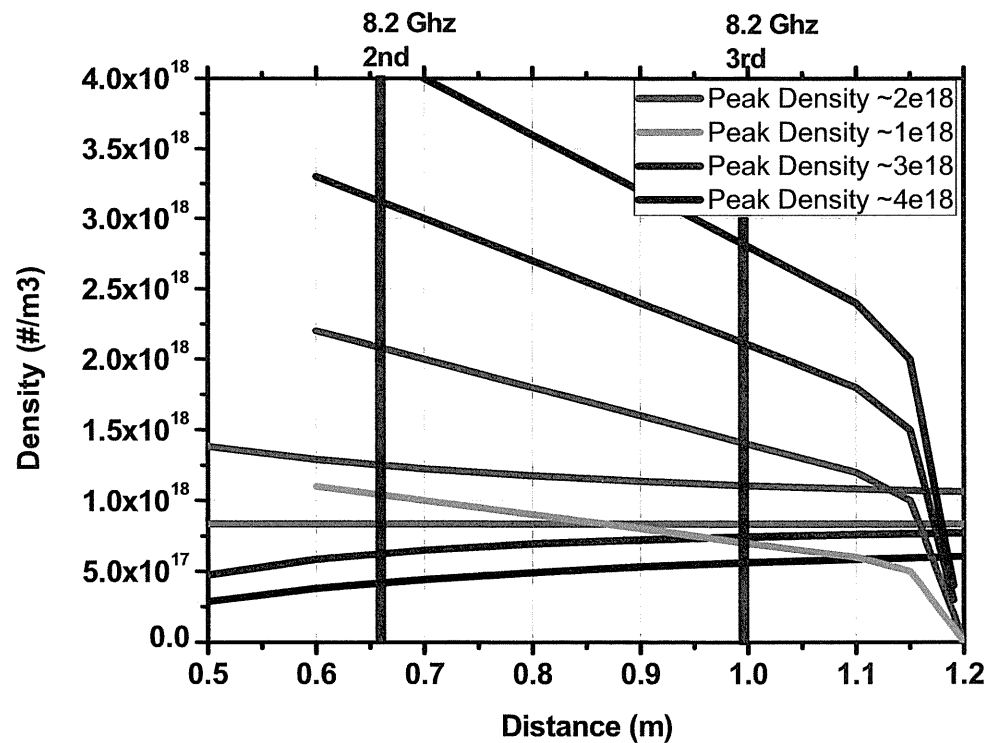
# Electron Bernstein wave (EBW) heating with direct XB mode conversion (MC) from low field side (LFS) injection in QUEST

- 1D Full wave simulation(Kim S. H., et al. Physics of Plasmas 21(6) (2014))
  - ✓ XB Mode conversion efficiency is calculated.
- QUEST Experiment with 400kW 28 GHz source(~2014)
  - ✓ ECH assisted Non-inductive Plasma current start-up at  $B_0 = 0.25$  T
  - ✓ Lower plasma density( $\sim 2E18$  #/m<sup>3</sup>) for the non-inductive plasma start-up with 28 GHz gives low direct XB MC efficiency of less than 5% for 8.2 GHz direct XB MC.
  - ✓ Some other means(ohmic) to increase plasma density of more than  $5E18$  #/m<sup>3</sup> are needed for sufficient LFS 8.2 GHz power coupling with direct XB MC as indicated



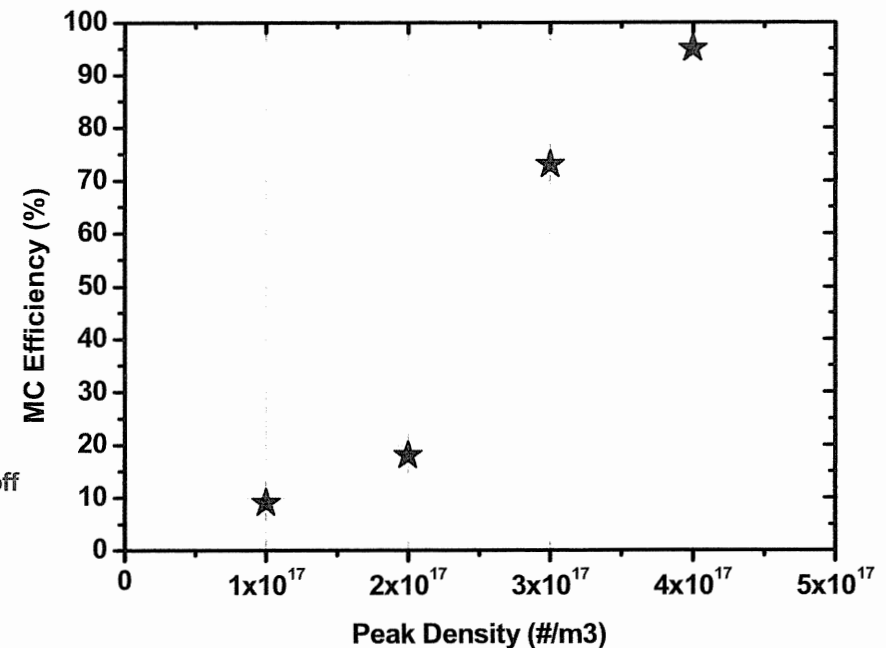
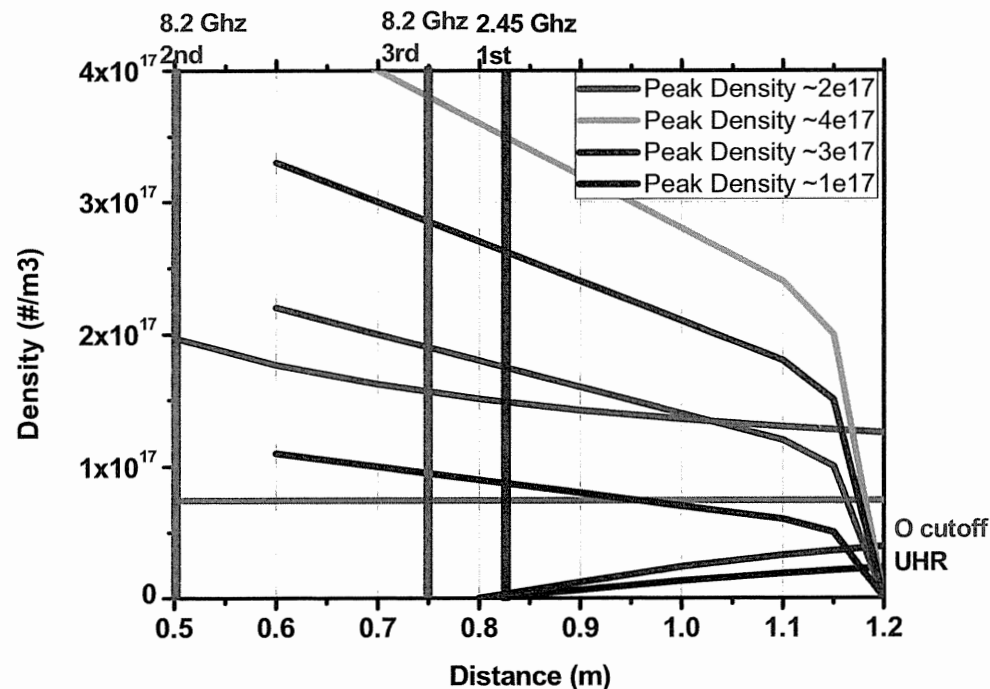
# EBW heating with direct XB mode conversion from LFS injection in QUEST

- QUEST Experiment with 200 kW 8.2 GHz MW source (First phase~2010)
  - ✓ ECH assisted Plasma current start-up with OH flux and 200 kW 8.2 GHz
  - ✓ Low toroidal field :  $B_0 = 0.14$  T at  $R_0 = 0.68$  m ( 8.2 GHz 1<sup>st</sup> harmonic : 0.33 m)
  - ✓ It is expected that if plasmas with high peak density of more than  $3e18$  #/m<sup>3</sup> are generated by any means such as ohmic heating (OH), direct XB MC efficiency will be increased significantly to form over-dense plasmas (profile assumption)



## EBW heating with direct XB mode conversion from LFS injection in QUEST

- QUEST Experiment with 200 kW 8.2 GHz MW & 30 kW 2.45 GHz (and OH if needed)
  - ✓ ECH assisted Plasma current start-up with 200 kW 8.2 GHz
  - ✓ 200 kW 8.2 GHz MW (and OH if needed) can be used to get sufficient plasma density for sufficient LFS 2.45 GHz power coupling with direct XB MC as indicated below.
  - ✓ Low toroidal field of  $B_0 = 0.11$  T at  $R_0 = 0.68$  m (2.45GHz for 1st harmonic and 8.2 GHz 3<sup>rd</sup> harmonic)
  - ✓ After plasmas are generated by 8.2 GHz MW, 2.45 GHz microwave power will be injected to the plasma and can generate over-dense plasmas with higher direct XB MC efficiency when the plasma density is formed to be over  $3E17$  #/m<sup>3</sup>.



# Schedule for experiment for XB mode conversion

- OH+8.2GHz
- 8.2GHz + 2.45GHz
- CHI + 8.2GHz

Which is suitable?

After checking, the experimental schedule will be fixed around the end of January and 1<sup>st</sup> week of February.

## 国際化推進共同研究概要

No.12

タイトル: Develop and improve EFIT code of the plasma equilibrium reconstruction for SSO operation and advanced physical study on QUEST

研究代表者: QIAN, Jinping

所内世話人: 花田 和明

概要:

# RESEARCH REPORT

Date Mar. 8 2018

Visiting scientist: (name) Jinping Qian

(position) Professor

(university / institute) Institute of Plasma Physics,

Chinese Academy of Sciences

Host scientist: (name) K. Hanada

(position) Professor

(university / institute) Kyushu University

Research period (remotely): (from) XX, 2017 (to) XX, 2017

**Research subject: Develop and improve EFIT code of the plasma equilibrium reconstruction for SSO operation and advanced physical study on QUEST**

Significant progress has been made in plasma equilibrium through the remote collaboration in the whole year of 2017, though without finding any good chance to communicate on-site.

A useful method for determination of the current and  $q$  profiles from Polarimeter-INTERferometer (POINT) diagnostic has been development, thus allowing the first time of equilibrium reconstruction of current-density profile. It is shown that the POINT measurements can be applied to improve the accuracy of core plasma current density and  $q$  profile on EAST. An example of comparison of reconstruction using magnetic measurements (red curves) against those reconstructed using magnetic and POINT data (blue curves) for an EAST lower single-null divertor equilibrium is shown in figure 1. Equilibrium reconstructions using POINT data are found to be consistent with sawtooth phenomena. The sensitivity of equilibrium reconstruction to POINT measurements indicates Faraday rotation provides important constraints for determining the current profile. Note that this result has been published in *Nucl. Fusion* 57 (2017) 036008.

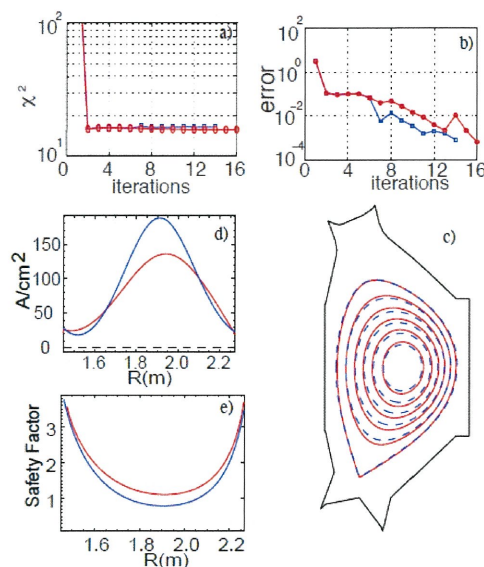


Figure 1 Reconstruction using magnetic measurements (red curves) against those

reconstructed using magnetic and POINT data (blue curves)

Secondly, an efficient technique for determining plasma equilibria with preset or constrained  $q$  profiles by solving the nonlinear GS equation is developed. The great advantage of this technique is that one can build a new equilibrium with a desirable  $q$  profile by directly presetting the  $q$  profile target. As an application for EAST, the method has been used to constrain the plasma equilibrium with measured locations of the  $q=1$  surfaces, which are extracted from ECE diagnostic, in addition to the external magnetic measurements (seen in figure 2). The magnetic reconstruction converges reasonably fast with two  $q=1$  surface constraints (High field side and low field side). This technique provides a useful method for constraining the plasma current density and  $q$  profiles when building the kinetic equilibrium for discharges that exhibit sawtooth behavior. Note that this result has been published in *Nucl. Fusion* 57 (2017) 084001.

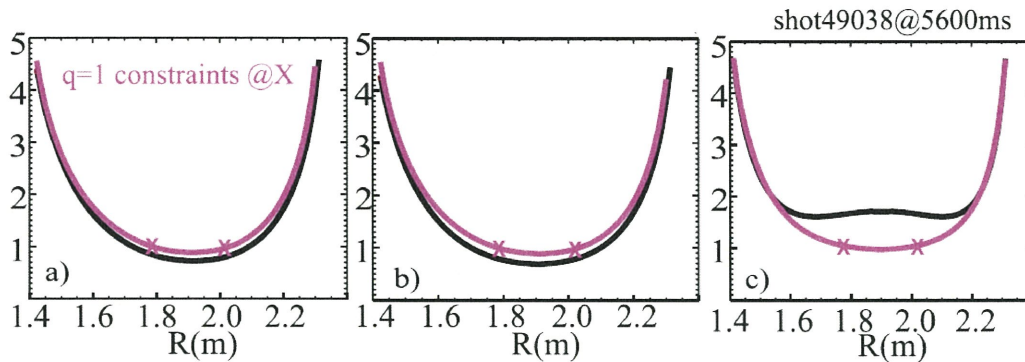


Figure 2 Comparison of reconstructed  $q$  profile using magnetic measurements only (black curves) against those reconstructed using magnetic measurements and  $q = 1$  constraints (pink curves), left to right:  $nF$  varied from 2 to 4.

(Signature) \_\_\_\_\_ J. Qian

(Name in print) \_\_\_\_\_ Jinping Qian